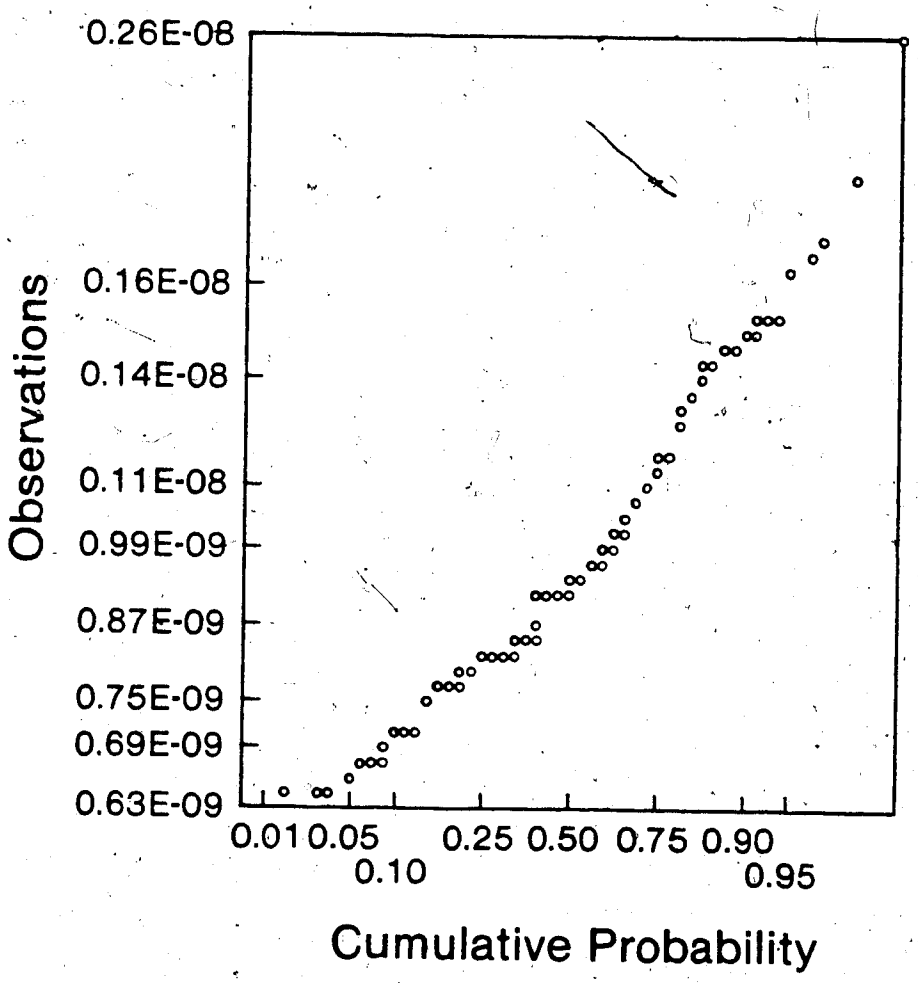

Figure 3.15 Log-normal probability plot

significance in most cases. Experimental results reported in ref. [51] confirm this trend.

(c) Fatigue threshold and comparison with experimental data.

Table 3.1 shows the material properties of the three metals used for comparison. One feature of the model is that it allows the estimation of the threshold stress intensity factor range. The number of fatigue elements in the damage zone depends on the applied stress intensity factor range. This is because the reversed plastic zone increases with the latter. If the applied stress intensity factor range is decreased, a stage is reached when the damage zone consists of only one fatigue element. At lower values of stress intensity factor range than this, the growth rate is insignificant since the damage accumulation outside the RPZ is negligible. This value of ΔK thus defines the threshold level of the stress intensity factor range, ΔKth. Table 3.2 shows the values of ΔK_{TH} determined this way compared to experimental data.

Figures 3.16 and 3.17 are the plots of the median growth rate from the simulation compared with published data, for 2219-T851-Aluminium alloy [21] and A516-Gr 70-Steel [45]. These results show good agreement with experimental data. In Fig. 3.18, the growth rate curve was plotted against ΔJ for both linear elastic tests and elastic-plastic tests for A533 B steel [5]. The linear elastic tests were in good agreement with the

Table 3.1 Material properties

Material Properties	2219 T851 Al	A516 Gr 70 Steel	A533 B Steel
b	-0.0756	-0.108	-0.085
c	-0.55	-0.506	-0.516
n'	0.121	0.19	0.165
σ'_o (MPa)	334.0	310.0	345.0
ε'_f	0.35	0.26	0.32
σ'_f (MPa)	613.0	900.0	869.0
E (GPa)	71.0	200.0	200.0
Δk_c (MPa $\sqrt{m}$)	30.0	200.0	140.0

Table 3.2 Threshold stress intensity factor range

MATERIAL	ΔK_{TH} (MPa $\sqrt{m}$)	
	PREDICTED	EXPERIMENT
1. 2219 T851 Al	3.0	3.0
2. A516 Gr 70 Steel	10.0	
3. A533 B Steel	7.0	8.0

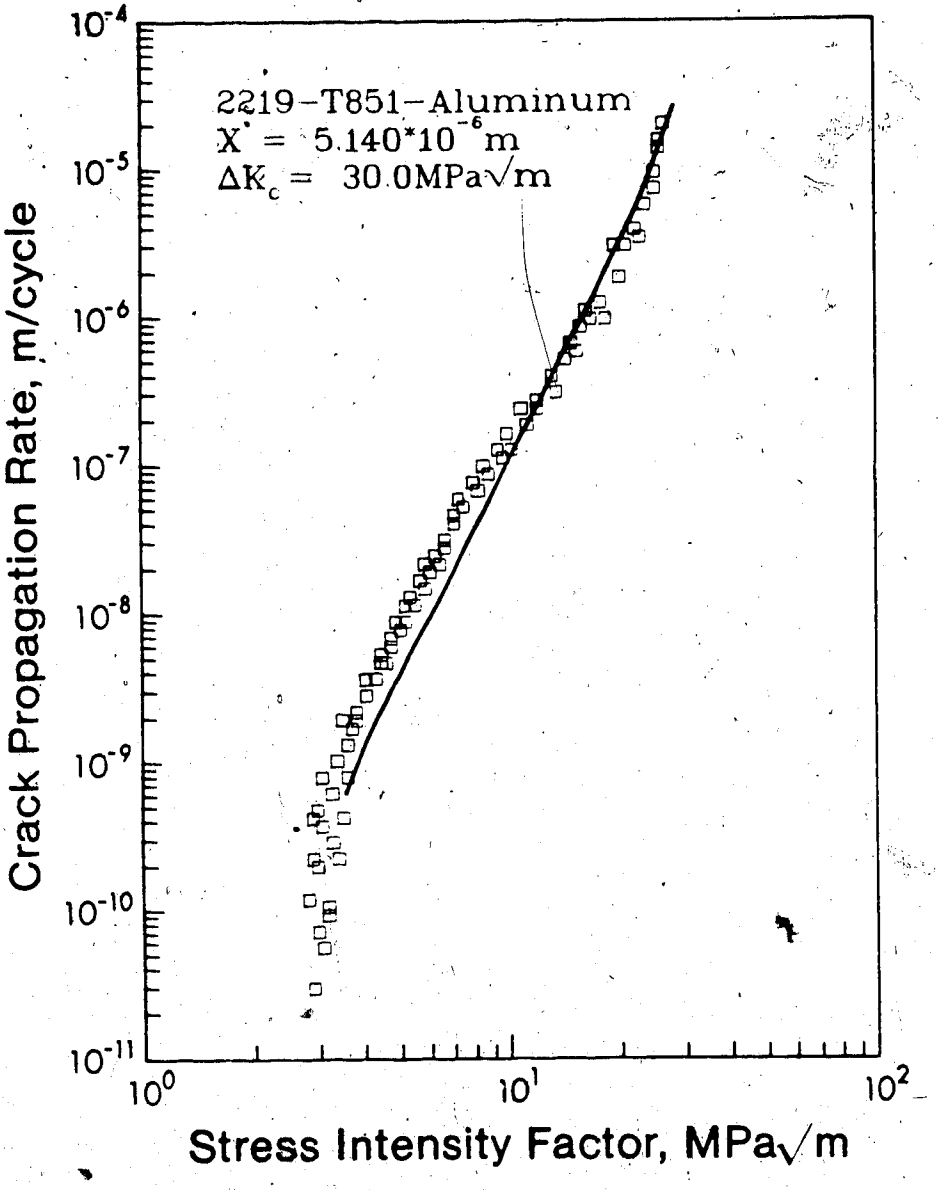

Figure 3.16 Comparison of experimental and predicted crack propagation rate vs stress intensity factor range

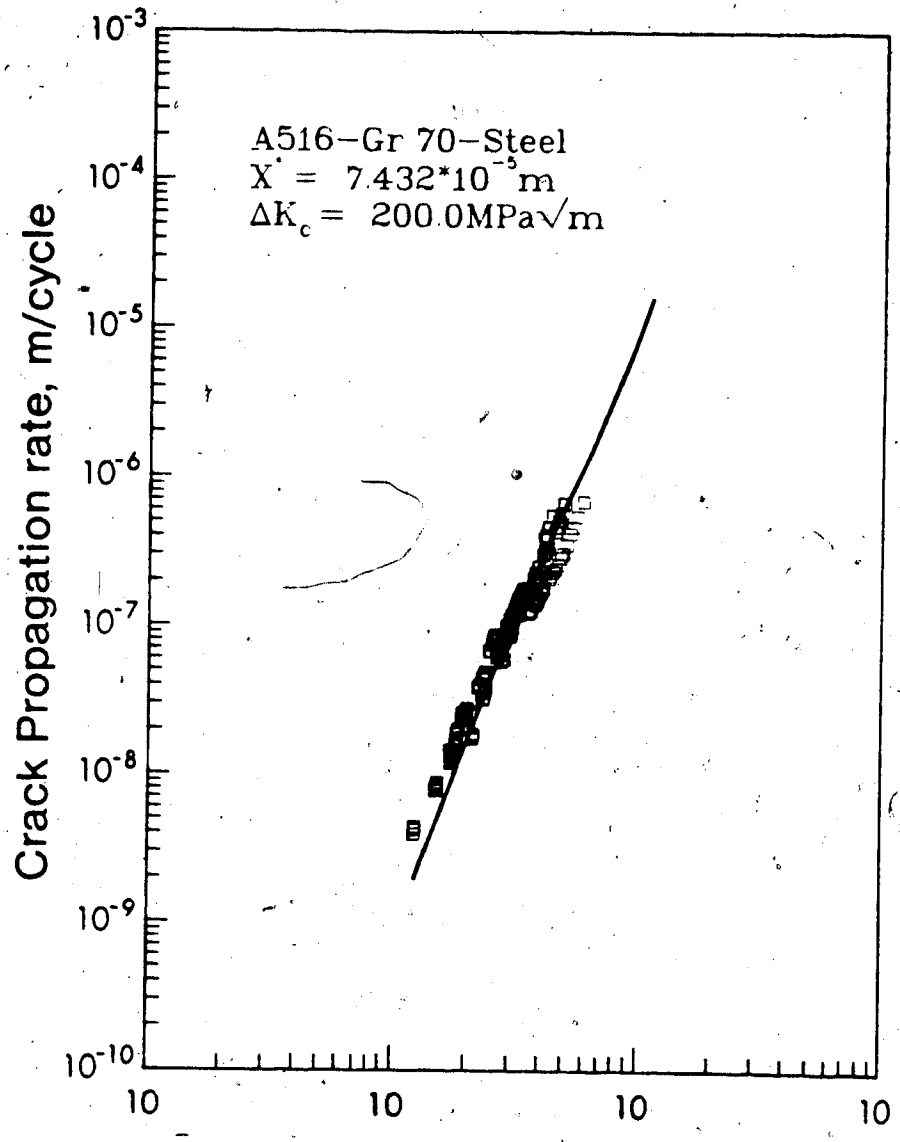

Figure 3.17 Comparison of experimental and predicted crack propagation rate vs stress intensity factor range

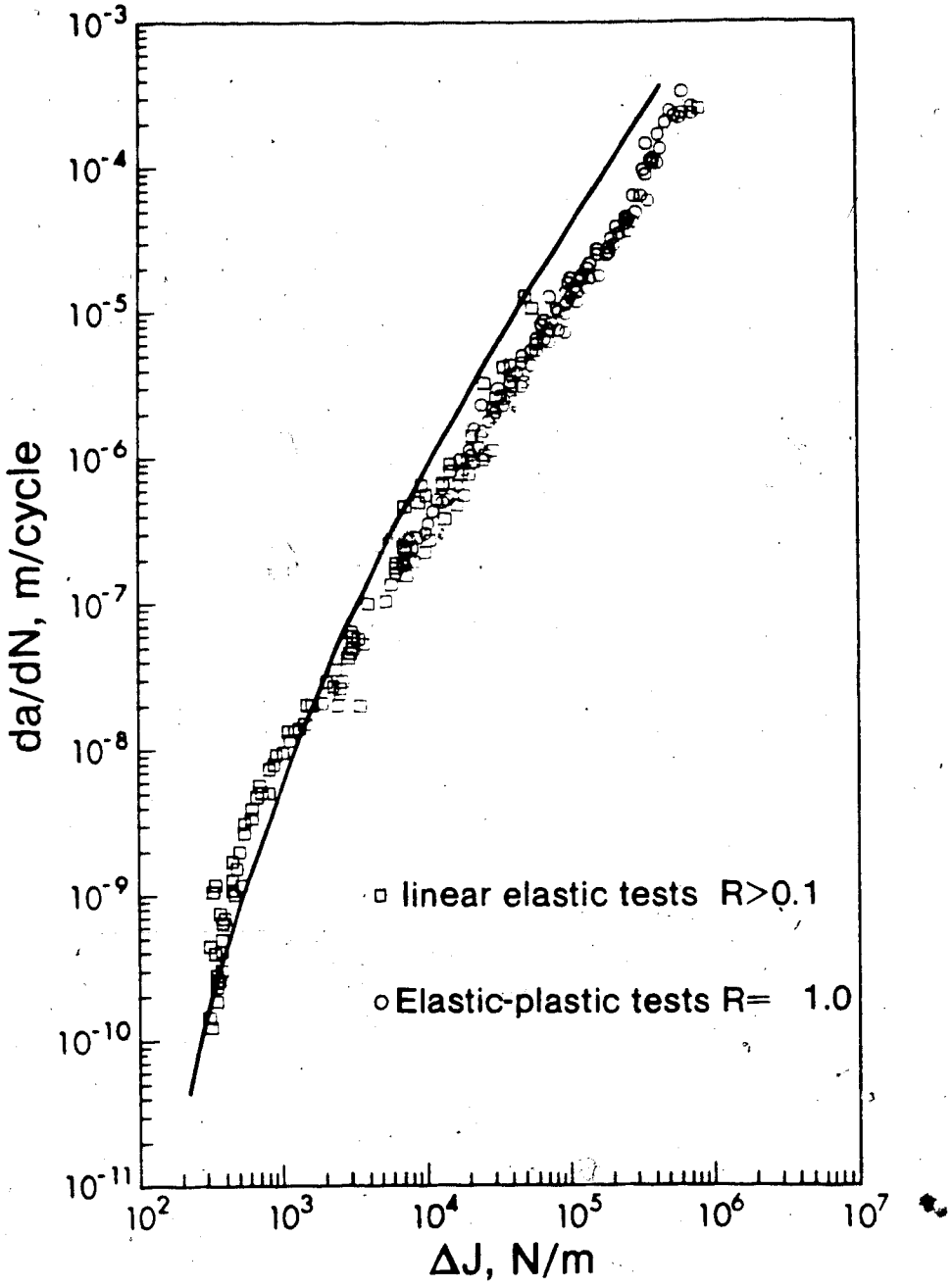

Figure 3.18 Comparison of experimental and predicted crack propagation rate vs cyclic J-integral (A533 B Steel)

model. However, the elastic-plastic tests deviated from the model by a factor of nearly two. This disparity is partly attributed to the definition of ΔJ used in plotting the experimental results, which were conducted at a different stress ratio from the linear elastic tests. ($R = -1$ for elastic-plastic, $R > 0.1$ for linear elastic). The definition of ΔJ in the elastic-plastic test is sensitive to the assumptions made on the stress ratio used.

For monotonic loading, see Dowling [5],

$$J = Je + Jp$$
$$= (\alpha W_e + \beta W_p)a \qquad 3.28$$

where J_e is the elastic J integral,

J_p is the plastic J integral,

a = half crack length,

α, β = constants derived in [3,4].

W_e = elastic work

W_p = plastic work

Dowling modified Eq. 3.28 in the following form:

$$\Delta J = (\alpha \Delta W_e + \beta \Delta W_p)a$$

The data in Fig. 3.18 are based on taking ΔW_e and ΔW_p as the full range of work done (Fig. 3.19). For fully reversed loading ($R = -1$), Mowbray [38] suggested a truncation of the applied ΔW_e and ΔW_p as shown to account for crack closure. Since crack closure was assumed to come

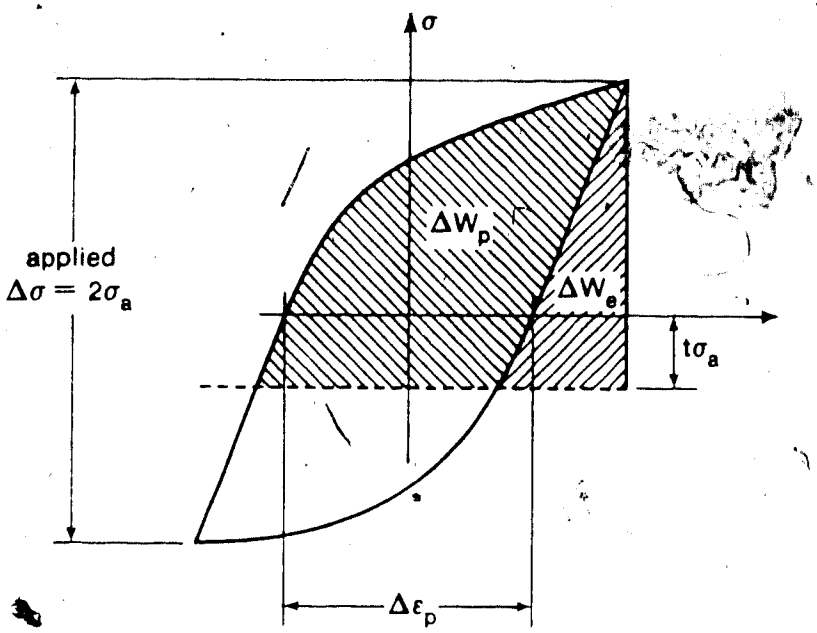

Estimation of crack ΔJ from stress strain hysteresis loops.

Figure 3.19 Estimation of crack ΔJ from stress-strain hysteresis loops

at a lower value of applied loading than the zero level, it was suggested in [38] that some (but not all) of the compressive portion should be included in the calculations of ΔW. The fraction suggested is $t = 1/3$. The works of Hudson [52] and Newman [53] suggest that only the positive part of the respective work done ($t=0$) should be applied. In the latter case, the value of the calculated ΔJ would be reduced by about half. This leads to the shifting of the elastic-plastic data (Fig. 3.18) to the left by a factor of 2.

(d)Concluding Remarks

Apart from the ability to predict the mean or median crack growth rate, this probabilistic simulation of fatigue crack growth leads to several fresh insights on the crack propagation phenomenon. Within the limits of the assumptions of the model, the simulation leads to a prediction of the threshold stress intensity range, below which the crack is not expected to grow. The simulation process also facilitates the consideration of the total damage history of the crack-tip elements. This way, the the historical damage is quantified. It is demonstrated that this quantity, often neglected by previous investigators, is of considerable significance. A Markovian treatment of probabilistic crack growth is thus inadequate unless a relationship can be found between the historical damage and the position of each fatigue element. Figures 3.7 to 3.12 show that such a relationship

in general depends on several factors. These include the applied loading, crack length and intrinsic material properties. This will be further complicated in the case of the elastic-plastic crack growth (large scale yielding) by the effects of plastic unloading discussed in the last section. The probabilistic distribution resulting from this model has been compared to three of the commonly used probability densities in the literature. No conclusive results can be drawn from probability plots alone. However the tendency toward the lognormal function in the Figs 3.13 to 3.15 cannot be ignored.

Chapter 4

DISLOCATION MODEL OF NON-LINEAR HARDENING

4.1 Introduction

In the preceding analysis, it has been necessary to know the distribution of stress and displacement (or strain) in the vicinity of the crack-tip, when the body in question is loaded cyclically. So far, in the literature, there has been no rigorous determination of these field quantities. As a result of this, the plastic superposition rule, extensively outlined by Rice [19] is widely used. This method was used to determine the cyclic fields in chapters 2 and 3. If the size of the crack in relation to the applied loading justifies the assumption of small scale yielding, for cyclic loading between σ_A and σ_B, the cyclic loading can be characterized by, ΔK, defined as:

$$\Delta K = \Delta\sigma\sqrt{\pi a} \qquad 4.1$$

where $\Delta\sigma = \sigma_B - \sigma_A$, so that,

$$\Delta K = K_B - K_A, \qquad 4.2$$

That is, the change in the stress intensity factor within the range.

However, the assumption of small scale yielding is very restrictive. Even with the far field stresses within

the elastic range, it is well known that the ratio of the plastic zone size to the crack length could be large enough to invalidate the results. Usually, in such a case, the J-integral would be a preferred quantity to characterize the crack-tip plasticity. The simple relationship between J-integral and K (or any other loading quantity), holds only in small scale yielding. Even for monotonic loading, analytical expressions for J-integral are difficult to obtain, except for small scale yielding. Goldman and Hutchinson [37] obtained closed form expressions for fully plastic materials and this has been used in conjunction with the small scale yielding results to provide some interpolated estimate for J-integral in the midrange [3,4]. The relevant weighting functions in this interpolation procedure were obtained using finite element methods.

Two problems arise when this interpolation method is applied to cyclic loading. Firstly, there is no equivalent of equation 4.2 for the J-integral. The cyclic J-integral cannot be obtained by simply subtracting the monotonic J-integral of the two levels of loading. Secondly, the weighting functions for the interpolation are available only for monotonic loading. Previous investigators [5, 38] have simply added the small scale yielding and fully plastic components of the J-integral in the midrange. Such a method is of doubtful validity unless the loading conditions are close to either small scale yielding or

full plasticity.

Using an extension of the BCS dislocation model, a method is described in this chapter that facilitates the direct evaluation of the J-integral. The extension involves the incorporation of work-hardening into the classical dislocation model in a more realistic way than previously attempted. We begin with a brief description of the Bilby and Swinden Linear Hardening Model. Then the conditions for the existence of a solution for the nonlinear work-hardening model presented are elucidated. The displacement integral equations are derived. The method of numerical solution is briefly described. Some of the significant results of the analysis are then presented.

(a) The Bilby and Swinden [18] model

This model is based on the dislocation model of BCS [17] already described in chapter 2. The main difference is in the assumption that the "friction stress", $\tau_1(x)$ resisting the motion of the dislocation into the material in question is now a function of position and of the plastic displacement at a given point;

$$\tau_1(x) = \tau_o + \omega\gamma_p(x) = \tau_o + \frac{\omega\phi(x)}{\alpha} , \qquad 4.3$$

where τ_o = minimum friction stress

$\gamma_p(x)$ is the plastic strain at distance x from the crack-tip,

$\phi(x)$ is the plastic displacement at the same point,

ω is a constant with the dimension of stress, and

α is a constant with the dimension of length.

Identifying τ_o (equation 4.3) with the material yield stress implies the modelling of a material, exhibiting a linear Hookean response for the states of stress within the yield point, and a linear hardening plastic behaviour for those outside. The plastic zone is, as in the BCS model, the extent of dislocation motion into the material.

The displacement field in this case was found by evaluating a linear integral equation where the unknown function also occurred inside the integral. The linearity of this problems allows a solution using linear algebra and matrix methods.

Even though the results show quite considerable change in the crack-tip displacement as a result of the incorporation of work-hardening, the plastic zone was not significantly affected. The only major problem observed was the occurrence of negative displacements ahead of the crack-tip when the plastic zone becomes too large.

4.2 A Non-Linear Work-Hardening Model

A bilinear stress-strain law in which the post yield behaviour of a material is considered linear can be considered as a first approximation. Such a choice is

attractive (as in the Bilby and Swinden model discussed earlier) because of the linearity of the resultant integral equations. However, in spite of this simplicity, there was no obvious closed form solution for the relevant plastic displacement field. The need to seek a fully numerical solution removes virtually all the advantages it may have over the more realistic (even though slightly complicated) modelling of the stress-strain law.

In the non-linear work-hardening model considered here, all the assumptions of the BCS model are retained except that the friction stress is considered to be of the form:

$$\tau_1(x) = \tau_0 \left(\frac{\gamma(x)}{\gamma_0}\right)^{n'} , \qquad 4.4$$

where, γ_0 is the yield strain, $\gamma(x)$ is the total strain at a distance x from crack centre, and n' is the hardening exponent in the modified Ramberg-Osgood stress-strain law. Since the plastic line represents states of plastic strain, the total strain at each point can be expressed as:

$$\gamma(x) = \gamma_p(x) + \gamma_0, \qquad 4.5$$

where $\gamma_p(x)$ is the plastic strain.

From equations 4.3 and 4.4, we have:

$$\tau_1(x) = \tau_0\left(\frac{\phi(x)}{\alpha\gamma_0} + 1\right)^{n'} = F\left(\phi(x)\right), \qquad 4.6$$

so that the post yield behaviour is non-linear of the Ramberg-Osgood type. Setting n'=0 in equation 4.6, the original BCS model is recovered, while n'=1, with a suitable choice of parameters, become identical with the linear hardening model of Bilby and Swinden.

For an external loading, resulting in a far field stress of magnitude τ^{∞}, equilibrium conditions requires that the sum of all forces (dislocation and external) acting at each location must vanish. Considering a continuous distribution of dislocations with density f(x), and Burger's vector b, this condition leads to:

$$\mathcal{R}\int_{-a}^{a} \frac{f(x')dx'}{x-x'} + \frac{P(x)}{A} = 0 , \qquad 4.7$$

where, $\mathcal{R}$ signifies that only the Cauchy Principal value of the singular integral is considered,

$$P(x) = \begin{cases} \tau^{\infty} & |x| < c \\ \tau^{\infty} - F(\phi(x)) & c \leq |x| \leq a , \end{cases}$$

and $A = \mu b/2\pi(1-\upsilon)$,

μ = rigidity modulus,

υ = poisson ratio,

c = crack length.

The plastic zone size, a, is an unknown in the equation 4.7 above. Its value can be evaluated by imposing a boundedness condition on the dislocation distribution density f(x), as will be discussed later.

In the next section, the conditions for the inversion of equation 4.7 will be described, and the integral equations for the displacement field will be formulated.

4.3 Conditions for Inversion of Equilibrium Equation

The inversion of the equilibrium equation 4.7 depends on the satisfaction of certain conditions related to the Holder inequality. We begin this section by presenting some definitions and lemmas to be invoked later in the inversion procedure.

(a) Holder Condition on a line segment [54,55]

Definitions and Lemmas

(i) Consider a function $\theta(t)$ defined on a line segment L, $\theta(t)$ is said to satisfy the Holder condition, or, equivalently, to belong to the class H, if for two arbitrary points of this line,

$$| \theta(t_2) - \theta(t_1) | < A | t_2 - t_1 |^{\lambda}, \qquad 4.8$$

where A (>0), is called the Holder constant, and, $0 < \lambda < 1$, is the Holder index.

(ii) If $\theta_1(t)$ defined on L, satisfies the Holder condition on every closed part of L not containing the

ends, and if, near any end, t=c, it is of the form,

$$\theta_1(t) = \frac{\theta(t)}{(t-c)^{\alpha}}, \quad 0 < \alpha \leq 1 \qquad 4.9$$

Given that θ belongs to the class H, then, $\theta_1(t)$ belongs to the class H* on L.

It is convenient at this point to state two lemmas which will be found useful later on:

Lemma 4.1

Consider f(t) defined on the line segment [c,a]. If f(x) is a positive monotonic decreasing function of t, then, the function,

$$\phi(x) \equiv -\int_x^a b\, f(t)dt, \quad c < x \leq a \qquad 4.10$$

belongs to class H, provided f(t) is bounded.

PROOF:

Consider $c < t_1 < t_2 < a$,

$$\phi_1(t_2) - \phi_1(t_1) = -b\int_{t_2}^{t_1} f(x)dx = b\int_{t_1}^{t_2} f(x)dx$$

$$\leq bf(t_1)\,|\,t_2 - t_1\,|\,. \qquad 4.11$$

Hence, $|\,\phi_1(t_2) - \phi_1(t_1)\,| \leq M\,|\,t_2 - t_1\,|^{\lambda}$, $M = bf(t_1)$

So that M is the Holder constant, and the index $\lambda=1$.

A corollary lemma follows immediately for f(t) monotonically increasing.

Lemma 4.2

Given that $\phi_1(t)$ is of class H on the line segment [c,a]. And given that $\phi_1'(t)$ and $\phi_2'(t)$ are both of the same sign (i.e., either both positive or both negative), if,

$$| \phi_2'(t) | < | \phi_1'(t) |, \text{ then}^3$$

$\phi_2(t)$ is also of class H in the same range.

PROOF:

$$| \phi_2(t_2) - \phi_2(t_1) | = \left| \int_{t_1}^{t_2} \phi_2'(t)dt \right|$$

$$= \int_{t_1}^{t_2} | \phi_2'(t) | dt < \int_{t_1}^{t_2} | \phi_1'(t) | dt.$$

$$\text{But } \int_{t_1}^{t_2} | \phi_1'(t) | dt = \left| \int_{t_1}^{t_2} \phi_1'(t)dt \right| = | \phi_1(t_2) - \phi_1(t_1) |. \qquad 4.12$$

Now, M and λ can be found such that,

$$| \phi_1(t_2) - \phi_1(t_1) | < M | t_2 - t_1 |^{\lambda}, \quad M > 0, \ 0 < \lambda \leq 1 \qquad 4.13$$

so that, from the above relationship,

$$| \phi_2(t_2) - \phi_2(t_1) | < M | t_2 - t_1 |^{\lambda}. \qquad 4.14$$

---

[3] The primes on the ϕ_i's here imply differentiation

(b) Inversion of the Equilibrium Equation

In order to obtain the dislocation distribution, the equilibrium equation 4.7 has to be inverted. The general solution of this problem has been given by Muskhelishvili [54,55]. The conditions to be satisfied are that, the dislocation $f(x)$ is of class H^*, and that $P(x)$ is of class H. With these conditions satisfied, if the Cauchy Principal value of the integrals exist at each point, then,

$$f(x) = \frac{2(1-\nu)}{\pi\mu b} \int_{-a}^{a} R(x,y)\, P(y)\, dy \,.$$

$$R(x,y) = \frac{1}{x-y} \sqrt{\frac{a^2-x^2}{a^2-y^2}} \,. \qquad 4.15$$

Guided by the solution of the BCS model (Chapter 2), it is reasonable to make the following assumptions about $f(x)$: Firstly, $f(x)$ is of class H^*, and secondly, $f(x)$ is a monotonic function of position in the two line segments [0,c], and [c,a]. These assumptions are based on the fact that for mild hardening, (moderate values of n') the function $f(x)$ should behave like $f_1(x)$ of chapter 2. Now, $f_1(x)$ is monotonic in the interval [c,a] and it is easily shown to be of class H^* in the vicinity of the crack-tip thus:

For any λ in the range, $0 < \lambda < 1$,

$$\lim_{x \to c^+} (x-c)^{\lambda} f_1(x) = \frac{\sigma_0}{\pi^2 A} \lim_{x \to c^+} (x-c)^{\lambda} \{ \cosh^{-1} \left| \frac{a^2 - c^2}{a(c-x)} + \frac{c}{a} \right| \quad 4.16$$

$$- \cosh^{-1} \left| \frac{a^2 - c^2}{a(c+x)} + \frac{c}{a} \right| \}$$

Using L'Hospital's rule, it follow that

$$\lim_{x \to c^+} (x-c)^{\lambda} f_1(x) = \frac{\sigma_0}{\pi^2 A} \lim_{x \to c^+} \left(\frac{2c}{x^2 - c^2} \sqrt{\frac{a^2 - c^2}{a^2 - x^2}} \right) / - \lambda (x-c)^{-\lambda - 1} = 0 \quad 4.17$$

where c^+ indicates an approach from the positive direction, so that $(x-c)^{\lambda} f_1(x)$ is bounded and continuous in the neighborhood of the crack-tip. Therefore, $f_1(x)$ belongs to the class H* in this neighborhood.

(c) Holder Condition for P(x)

Now, define,

$$\phi(x) \equiv - \int_x^a b \, f(t) dt, \quad c < x \leq a, \quad 4.18$$

By Lemma 4.1, $\phi(x)$ belongs to the class H in the open interval, (c,a]. It follows easily that any linear function of $\phi(x)$ also belongs to class H. In particular, the function

$$\phi_1(x) \equiv \frac{\mu\phi(x)}{\alpha} \qquad 4.19$$

where μ and α are constants.

We now proceed to show that non-linear function

$$\phi_2(x) = \tau_0 \left\{\left(\frac{\phi(x)}{\alpha\gamma_0} + 1\right)^{n'} - 1\right\} \qquad 4.20$$

satisfies all the conditions of Lemma 4.2. Differentiating Eq. 4.20, we obtain,

$$\frac{d\phi_2(x)}{dx} = \frac{n'\tau_0}{\alpha\gamma_0}\left(\frac{\phi(x)}{\alpha\gamma_0} + 1\right)^{n'-1} \frac{d\phi(x)}{dx} \qquad 4.21$$

From the relationship 4.19 and noting that $\mu = \tau_0/\gamma_0$, the above equation can be used to obtain,

$$\frac{d\phi_2(x)/dx}{d\phi_1(x)/dx} = n'\left(\frac{\phi(x)}{\alpha\gamma_0} + 1\right)^{n'-1} \qquad 4.22$$

By definition, $0 < n' < 1$, and $\phi(x)$ is positive. Therefore, the right hand side of equation 4.22 is always positive. This immediately shows that $\phi_1'(x)$ and $\phi_2'(x)$ are of the same sign.

Rewriting equation 4.22,

$$\frac{\phi_2'(x)}{\phi_1'(x)} = \frac{n'}{\left(\frac{\phi(x)}{\alpha\gamma_0} + 1\right)^{1-n'}} \qquad 4.23$$

The numerator on the right hand side of equation 4.23 is less than unity but the denominator is always greater than unity as long as $\phi(x)/\alpha\gamma_0$ is positive. This is always the case. It therefore follows that,

$$\left| \phi_2'(x) \right| < \left| \phi_1'(x) \right| \qquad 4.24$$

In which case, we have shown that $\phi_2(x)$ is of class H for $|x|$ the interval $(c,a]$.

In the open interval $|x| < c$, $P(x)$ in equation 4.7 meets the Holder condition. In the open interval,

$$c < |x| \leq a,$$

$$P(x) = \tau^{\infty} - \tau_1(x) = \tau^{\infty} + \tau_0 - \phi_2(x), \qquad 4.25$$

using the notation in this section. It is clear that the Holder condition is also satisfied in the open interval $(c,a]$. In order to include the discontinuity at $x=c$, it is convenient to modify the function $P(x)$ slightly by approximating the step at $x=c$ by a linear function in the interval $[c-\delta, c+\delta+\epsilon]$ as shown in Fig. 4.1. In the limit

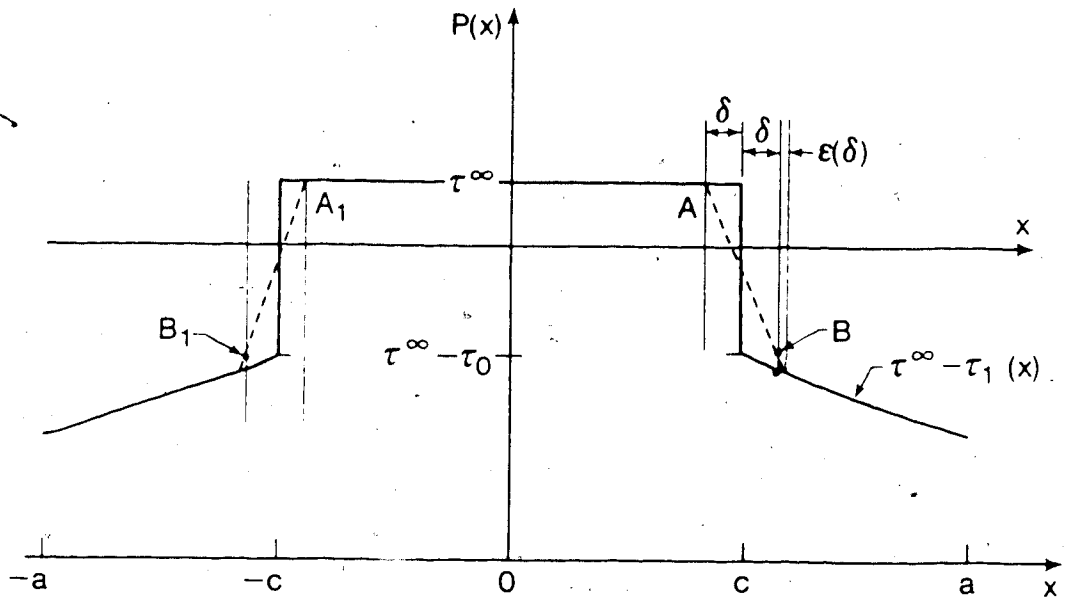

$A = (c-\delta, \tau^{\infty})$, $A_1 = (-c+\delta, \tau^{\infty})$

$B = (c+\delta, \tau^{\infty}-\tau_1)$, $B_1 = (-c-\delta, \tau^{\infty}-\tau_0)$

Figure 4.1 Holder condition for a step function

as $\delta \to 0$, the function $P_2(x)$ becomes identical with the function $P(x)$. Moreover, the inversion problem in question, using $P_2(x)$ converges to a solution equivalent to what would be obtained if $P(x)$ had been used in the first place. A justification for this is discussed in the rest of this section.

Consider the straight line AB (or A'B') in Fig. 4.1. It is convenient to divide the region $|x| \leq a$ into the following sub-intervals

$$
\begin{aligned}
&I_1; \quad |x| \leq c - \delta \\
&I_2; \quad c + \delta + \varepsilon \leq |x| < a \\
&I_3; \quad c - \delta \leq x \leq c + \delta + \varepsilon \\
&I_4; \quad c - \delta - \varepsilon \leq x \leq -\varepsilon - \delta
\end{aligned}
\tag{4.26}
$$

where the parameters δ and ε are as defined in the Figure. As a modification of the function $P(x)$, define $P_2(x)$, as

$$
P_2(x) = \begin{cases} P(x), & x \in I_1, I_2 \\ \tau^{\infty} - (\tau_0/2) - (|x| - c)\,\tau_0/2\delta, & x \in I_3, I_4 \end{cases}
\tag{4.27}
$$

Now, for any finite values of δ, and $\varepsilon(\delta,n')$, $P_2(x)$ satisfies Holder condition in the entire range, $|x| < a$. Using $P_2(x)$ instead of $P(x)$ in 4.7, which can be inverted as in 4.23 to give:

$$f(x) = \frac{2(1-\upsilon)}{\pi\mu b} \int_{I_1 U I_2 U I_3 U I_4} R(x,y)\, P_2(y)dy \qquad 4.28$$

$$= \frac{2(1-\upsilon)}{\pi\mu b} \left\{ \int_{I_1 U I_2} R(x,y)\, P_2(y)dy + \int_{I_3 U I_4} R(x,y)\, P_2(y)dy \right\}$$

where

$$R(x,y) = \frac{1}{x-y} \sqrt{\frac{a^2 - x^2}{a^2 - y^2}}\,. \qquad 4.29$$

For any point $x \neq c$, however close to the crack-tip c, δ_o can be found satisfying:

$$|\, x-c \,| > 2(\delta_o + \varepsilon\,(\delta_o,n')) > 2(\delta + \varepsilon(\delta,n')) \qquad 4.30$$

near the crack-tip closer to the point x in question.

Given that $y \in I_3 U I_4$, then y satisfies,

$$|\, y-c \,| < \delta + \varepsilon(\delta,n'). \qquad 4.31$$

Using 4.30 and 4.31, therefore, it follows that,

$$| x-y | = | x - c - (y-c) | > | x-c | - | y-c | > \delta + \varepsilon(\delta,n'). \qquad 4.32$$

In which case, the second term on the right hand side of equation 4.28 is free of singularity, for all values of δ satisfying 4.30. Moreover, from the construction in Fig. 4.1, it is clear that if δ approaches zero, $\varepsilon(\delta,n')$ will also approach zero. But the integral of any finite function vanishes as the domain of integration tends to zero. It follows therefore, that,

$$\lim_{\delta \to 0} P_2(x) = P(x) \qquad 4.33$$

and,

$$\lim_{\delta \to 0} \frac{2(1-\upsilon)}{\pi\mu b} \int_{I_1 \cup I_2 \cup I_3 \cup I_4} R(x,y)\, P_2(y)dy$$

$$= \frac{2(1-\upsilon)}{\pi\mu b} \int_{-a}^{a} R(x,y)\, P(y)dy \qquad 4.34$$

So that, even though P(x) does not satisfy the Holder conditions, a supplementary function $P_2(x)$ can be found belonging to the class H, which converges to the function P(x) in the limit as just described.

A similar argument was used by Swinden [55] for the simpler case when the value of P(x) is constant in the whole range with the exception of a step at the point x=c.

4.4 Displacement Integral Equations

Having established the conditions of validity of the inversion of Eq. 4.33, we proceed in this section to generate the integral equations for the plastic displacement function and the relevant boundary condition. The requirement that the dislocation density function f(x) be bounded at the end points ±a, similar to the condition in Eq. 2.19, is:

$$\int_{-a}^{a} \frac{F(x')dx'}{[(x'-a)(x'+a)]^{1/2}} = 0. \qquad 4.35$$

In the case of this non-linear hardening model, the relevant function F(x) is the function P(x) defined in 4.7. In which case, 4.35 becomes,

$$\int_{-a}^{-c} \frac{\tau^{\infty} - \tau_1(x')}{(a^2 - x'^2)^{1/2}} dx' + \int_{-c}^{c} \frac{\tau^{\infty} dx'}{(a^2 - x'^2)^{1/2}} + \int_{c}^{a} \frac{\tau^{\infty} - \tau_1(x')}{(a^2 - x'^2)^{1/2}} dx' = 0 \qquad 4.36$$

which after rearranging, and substituting from 4.6, becomes,

$$\int_{-c}^{c} \frac{\tau^{\infty} dx'}{(a^2 - x'^2)^{1/2}} + \left(\int_{-a}^{-c} + \int_{c}^{a}\right) \frac{\tau^{\infty} - \tau_o\left\{\frac{\phi(x')}{\alpha\gamma_o} + 1\right\}^{n'}}{(a^2 - x'^2)^{1/2}} dx' = 0 \qquad 4.37$$

Unfortunately, 4.37 does not lead to a closed form relationship between the applied loading, τ^{∞} and the extent of plasticity, a, like in 2.20. In the present case, the plastic displacement $\phi(x)$ at each position must be found, by integrating 4.15, before solving 4.37. The plastic displacement at any point x,

$$\phi(x) = b \int_{x}^{a} f(x') \, dx' \qquad 4.38$$

where a is the plastic zone extent closer to the point x. Substituting for f(x) from 4.15, we obtain,

$$\phi(x) = \frac{2(1-\upsilon)}{\pi\mu} \int_{-a}^{a} \int_{x}^{a} b \, R(x',y) \, P(y) \, dy \, dx'. \qquad 4.39$$

From equation 4.7, P(x) can be rewritten,

$$P(x) = \begin{cases} \tau^{\infty} & |x| < c \\ \tau^{\infty} - \tau_o\left\{\left(\frac{\phi(x)}{\alpha\gamma_o} + 1\right)^{n'} - 1\right\} & c < |x| < a \end{cases} \qquad 4.40$$

$$= P'(x) - P''(x) \ .$$

so that, 4.39 becomes,

$$\phi(x) = \frac{2(1-\nu)}{\pi\mu} \left\{ \int_{-a}^{a} \int_{x}^{a} bR(x',y)\ P'(y)\ dydx' \right.$$

$$\left. - \int_{-a}^{a} \int_{x}^{a} bR(x',y)\ \tau_0 \left[\left(\frac{\phi(y)}{\alpha\gamma_0} + 1 \right)^{n'} - 1 \right] dydx' \right. \qquad 4.41$$

Clearly, P' in the above equation is the same function as P(x) in equation 2.18. We can write, therefore,

$$\phi(x) = \phi_0(x) - B \int_{c}^{a} \tau_0 \left\{ \left(\frac{\phi(y)}{\alpha\gamma_0} + 1 \right)^{n'} - 1 \right] dy \int_{x}^{a} [R(x',y) + R(x', -y)]dx' \qquad 4.42$$

where $B = 2(1 - \upsilon)\gamma_0/\pi$

Writing,

$$K(x,y) = \int_{x}^{a} [R(x';y) + R(x';-y)]dx', \qquad 4.43$$

equation 4.42 becomes,

$$\phi(x) = \phi_o(x) - B \int_c^a \left(\left(\frac{\phi(y)}{\alpha \gamma_o} + 1 \right)^{n'} - 1 \right) K(x,y)\, dy \qquad 4.44$$

It can be shown (see appendix) that,

$$K(\quad = \cosh^{-1} \left| \frac{a^2-x^2}{a(x-y)} + \frac{x}{a} \right| + \cosh^{-1} \left| \frac{a^2-x^2}{a(x+y)} + \frac{x}{a} \right| - 2 \sqrt{\frac{a^2-x^2}{a^2-y^2}} \qquad 4.45$$

and, $\phi_o(x)$ is given by,

$$\frac{1}{B} \phi_o(x) = (x+c) \cosh^{-1} \left| \frac{a^2-x^2}{a(x+c)} + \frac{x}{a} \right| - (x-c) \cosh^{-1} \left| \frac{a^2-x^2}{a(c-x} + \frac{x}{a} \right|$$

Equations 4.44 and 4.37 can be treated therefore as simultaneous integral equations in the two unknowns, $\phi(x)$, and a. In 4.37 the unknown quantity, a, appears as a limit in one of the integrals, as well as under the integral signs. There is no obvious analytical solution to these equations. The next section of this chapter deals with the procedure used in arriving at an optimal numerical solution.

4.5 Numerical Solution of the Work-Hardening Equations

(a) General Procedure

The displacement function has been expressed in the last subsection in the form of a Fredholm Integral Equation of the second kind (Eq. 4.44) and a boundary condition (also expressed as an integral), Eq. 4.37. The method chosen to solve this problem belongs to the general class called "expansion methods". As already discussed in chapter 2 (section 2.6), a more familiar procedure is the quadrature method, where the integral in the equation in question is changed, using standard quadrature formulae, to an algebraic expression in terms of specific values of the kernel function and the unknown function in question. This is basically an expansion method, but with the basis functions limited to the kernel of the integral equation. Since the kernel function in Eq. 4.44 is singular, it is found desirable that there be freedom to choose basis functions other than the kernel function itself.

In general, we can choose to represent the unknown function $\phi(x)$ in 4.44 as a linear combination of certain prescribed functions, thus:

$$\phi(x) = \sum_{i=0}^{n} \alpha_i \phi_i(x), \qquad 4.46$$

the α_i's are the parameters to be estimated and n is the number of basis functions. It is usual to choose for the α_i's, functions that are independent of any unknown

parameters. Polynomials in x are common examples. If the friction stress is, for instance, as given in Eq. 4.3, then 4.44 will be linear. In this case, the choice of polynomials, or other functions independent of the α_i's in Eq. 4.46 will lead to a set of linear equations, which can be solved by standard matrix methods. However, when the friction stress is non-linear (Eq. 4.6), choice of α_i's independent of unknown parameters will still not give linearity. In this case, the choice of non-linear combinations of functions of the form,

$$\phi(x) = \sum_{i=1}^{n} \alpha_i \phi_i(\underline{\alpha}, x), \qquad 4.47$$

where $\underline{\alpha}$ is the vector $\{\alpha_i\}$, and the ϕ_i's are arbitrary functions, does not necessarily lead to greater complications because the resulting equations will always be non-linear anyway. In the next subsection, methods of singularity removal including the use of the basis functions to eliminate the kernel singularity, will be treated.

(b) Singularity Removal Method

In the case of linear hardening, n'=1 the friction stress has the form of Eq. 4.3. The simplest set of basis functions are polynomials. If the functions ϕ_i's in Eq. 4.46 are polynomials or any elementary functions, we can choose a vector x_j, j = 1, . . ., m, where x_j is any point in the domain [c,a]. A substitution in the equation 4.44

results in the m equations:

$$\eta_j \equiv \eta(x_j) \equiv \phi(x_j) - \phi_o(x_j) + B \int_c^a \frac{\mu\phi(y)}{\alpha} K(x_j,y)dy, \qquad 4.48$$

where $\phi(x_j) = \sum_{i=1}^{n} \alpha_i \phi_i(x_j)$

$$\phi(y)K(x_j,y) = \sum_{i=1}^{n} \alpha_i \phi_i(y)K(x_j,y) \quad , \qquad j=1, \ldots, m \qquad 4.49$$

and, η_j is the residual at the point x.

As long as the function ϕ_i's do not involve the parameters α_i, Eq. 4.48 is linear. The solution method used depends on the choice of the number of points, m. For a unique solution to exist

$$m>n \qquad 4.50$$

When m=n, there is the same number of solutions and unknowns. An attempt can be made to solve the linear algebraic equations,

$$\eta_j = 0, \quad j=1, \ldots, n \qquad 4.51$$

The condition for existence of a solution to Eq. 4.51 is that the matrix whose i,j^{th} term, A_{ij} is defined by,

$$A_{ij} = \phi_i(x_j) + B \int_c^a \frac{\mu}{\alpha} \phi_i(y) K(x_j,y)dy \qquad 4.52$$

has a unique inverse.

Within the range [c,a] of the integral on the RHS of Eq. 4.52, there are singularities at points x=y, and y=a. One method available for removing the latter singularity is to choose the functions ϕ_i's that satisfy:

$$\phi_i(x) = (a^2 - x^2)^t \xi_i(x), \quad t \geq 3/2 \qquad 4.53$$

provided that $\xi_i(x)$ is bounded, and has bounded derivatives in the domain [c,a]. It can be shown then that,

$$\lim_{y \to a} \phi_i(y)\, K(x_i,y) \qquad 4.54$$

exists. The other kernel singularity, x=y, is an integrable one. The following procedure was used in integrating around it.

Consider the function F(y), and let K(x,y) have a singularity at x=y in the integral,

$$\int_c^a F(y)\,K(x,y)\,dy = \int_c^a \Big(F(y) - F(x)\Big)K(x,y)dy + F(x)\int_c^a K(x,y)dy \qquad 4.55$$

as $x \to y$, $K(x,y) \to \infty$. But the quantity $F(y)-F(x)$ approaches zero. The first term in the expression in 4.55 vanishes in the limit, otherwise, the integral does not exist [56]. At the same time, if $K(x,y)$ has a closed form integral, as it indeed does in this case, then the expression 4.55 can be evaluated by standard procedures. This way, the second kernel singularity can be avoided.

In the general case, $n' \neq 0,1$, in place of Eq. 4.48, we have;

$$\eta_j = \phi(x_j) - \phi_o(x_j) + B\tau_o \int_c^a \{(\frac{\phi(y)}{\alpha\gamma_o} + 1)^{n'} - 1\} K(x_j,y)dy \qquad 4.56$$

that is,

$$\eta_j = \sum_{i=1}^{n} \alpha_i \phi_i(\underline{\alpha},x_j) - \phi_o(x_j) + B\tau_o \int_c^a \{(\frac{\sum_{i=1}^{n} \alpha_i \phi_i(\underline{\alpha},y)}{\alpha\gamma_o} + 1)^{n'} - 1\} K(x_j,y)dy \qquad 4.57$$

so that the functions η_j's are non-linear in the unknown parameters. There is, therefore, no obvious advantage in choosing $\varphi(x)$ as a linear combination of functions. We

return to this point later, but now, we can discuss the problem of singularity removal due to the nonlinearity.

The singularity at $x_i=y$ can still be removed as demonstrated in Eq. 4.55. However, functions satisfying the condition in Eq. 4.53 are no longer guaranteed to ameliorate the singularity at y=a. Since the latter is at a fixed point, at the end of the domain of integration, it is found convenient to avoid the point y=a by selecting the points x_j in the open interval [c,a). That is, we go as near to a as we may desire, but avoid using the point $x_j=a$ itself.

(c) Numerical Solution

The following perturbation of the elastic-perfectly plastic solution (Eq. 2.22),

$$\phi(x) = \alpha_1(x+c)\cosh^{-1}\left[(1+|\alpha_2|)\left|\frac{a^2-x^2}{a(c+x)}+\frac{x}{a}\right|\right] - \alpha_3(x-c)\cosh^{-1}\left[(1+|\alpha_4|)\left|\frac{a^2-x^2}{a(c-x)}+\frac{x}{a}\right|\right] + \alpha_5 e^{-\alpha_6(x/a)} + \alpha_7 e^{-\alpha_8(x^2/a^2)} \qquad 4.58$$

with an exponential and Gaussian background (the last two terms respectively) is used as the approximation function. Since there are eight unknown parameters, in principle, only eight equations are needed to evaluate them. However, it was found more accurate to choose more points x_j than

eight, so that the resulting set of equations (of the type of Eq. 4.57) becomes a set of overdetermined non-linear equations. This approach is chosen because, in this way, accuracy of the procedure can be improved by choosing more points provided the point $x_j=a$ and the other singularity ($x_j=y$) in Eq. 4.57 are avoided as already described. In the calculations presented in this chapter, twenty equally spaced points were chosen, and the resulting equations were solved via a non-linear least squares method. The sum of square residuals,

$$\sum_{j=1}^{20} r_j^2 \qquad 4.59$$

was minimized using the IMSL [57] subroutine based on a derivative-free optimization method for non-linear least squares. The method used there is based on the Levenberg-Marquardt algorithm. The optimization routine does not require the computation of gradient vector or the Hessian matrix. One only needs to supply an initial estimate of the vector $\{\alpha_i\}$. The initial estimate used was (1,0,1,0,0,1,0,1). Using this vector in Eq. 4.58, the initial estimate corresponds to the elastic-perfectly plastic solution (Eq. 2.22). The boundary conditions 4.37 was included in this way: starting from a reasonable initial estimate a_0 of the parameter a, for any value a_k, the residual at the k^{th} iteration,

$$r_k = \int_{-c}^{c} \frac{\tau^{\infty}\, dx'}{\left(a_k^2 - x'^2\right)^{1/2}} + \left(\int_{-a_k}^{-c} + \int_{c}^{a_k} \right) \frac{\tau^{\infty} - \tau_0 \left\{ \frac{\phi(x')}{\alpha \gamma_0} + 1 \right\}^{n'}}{\left(a_k^2 - x'^2\right)^{1/2}} \qquad 4.60$$

is found, using the value of the vector $\{\alpha_i\}_k$ corresponding to this optimization. It turns out that the choice of a_0, close to the elastic-perfectly plastic value (Eq. 2.20), gives r_k close to zero. By using different values of a_k in an iterative scheme, the magnitude of r_k can be made as small as possible, giving a good estimate of a. Another way to solve this problem is to solve the integral equation 4.37 directly for each optimal value of the vector $\{\alpha_i\}_k$. However, the computational requirement for this solution make it unattractive.

Apart from converging to an optimal (minimal) value of the sum in 4.59, the final solution is tested at each optimization point. When the residuals, N_j's are of a lower order of magnitude than the function, $\sum_{i=1}^{n} \alpha_i \phi_i(\underline{\alpha}, x_j)$ the vector $\{\alpha_i\}_k$ is taken as a sufficiently close estimate of the unknown parameter vector. Various values of the hardening exponent were considered in the range $0 \leq n' \leq 0.2$. The iterative method described here converged in all cases for applied stress values up to 0.6τ_0. For values of the hardening exponent higher than this range, and/or higher values of the applied loading, the convergence rate is slow, and both the sum of squares errors as well as the individual errors become large. In

some cases, the latter has a magnitude comparable to the estimated displacement function.

The optimal vector $\{\alpha_i\}$ obtained by the method described can then be substituted in Eq. 4.58 to obtain the plastic displacement $\phi(x)$ as a function of distance from the crack centre. The stress distribution, $\tau_1(x)$ can be obtained from $\phi(x)$ using Eq. 4.6. Another important quantity to be evaluated is the J-integral. By definition,

$$J = \int_{\Gamma} W dy - T_m \frac{\partial u_m}{\partial x} ds \qquad 4.61$$

where Γ is a suitable integration path around the crack-tip plastic zone, u_m is the displacement vector,

$W = \int_0^{\varepsilon_{k\ell}} \sigma_{k\ell}\, d\varepsilon_{k\ell}$ the strain energy density,

and, T_m is the traction vector.

In the dislocation model, the simplest path of integration is the upper and lower surfaces of the plastic zone. Along the plastic line, $dy=0$, so that the first term in the integral (Eq. 4.61) vanishes. Also, $ds=dx$.

Equations 4.6 and 4.61 lead to:

$$J = -\int_c^a \tau_1(x) \frac{d\phi(x)}{dx} dx \qquad 4.62$$

Since $\phi(x)$ is the relative plastic displacement at point x

between the two surfaces constituting the integration path Γ, so that,

$$J = -\tau_0 \int_c^d \left\{\frac{\phi(x)}{\alpha\gamma_0} + 1\right\}^{n'} d\phi(x) \qquad 4.63$$

and, now, $\phi(x)$ can be obtained from Eq. 4.58.

4.6 Results and Discussion

In the range of applied loading $0 \leq \tau^{\infty} \leq 0.6\tau_0$, the plastic displacement $\phi(c)$ at the crack-tip varied widely. In Table 4.1, the spread of values can be seen to span over two orders of magnitude. A linear plot of these values will give the impression that there is no change in displacement over the range of values between $0.0 < \tau^{\infty} \leq 0.4\tau_0$. These values are therefore plotted on a logarithmic scale as shown in Fig. 4.2. Here, the displacement is made dimensionless by dividing it by the quantity $\alpha\gamma_0$. As expected, the displacement increases rapidly with the applied far field loading. There is a reduction in the crack-tip displacement when the hardening exponent n' is increased. Even though this has been attenuated by the logarithmic plot, the trend is consistent with expectations.

Figure 4.3 depicts the variation in the dimensionless crack-tip stress, $\tau_1(x)/\tau_0$ with the applied loading, for

Table 4.1 Variation in crack-tip displacement due to external loading and hardening

τ/τ_o \ n'	0.0005	0.05	0.10	0.125	0.1667	0.200
.0500	0.13759	0.13751	0.13747	0.13742	0.13738	0.13731
.1000	0.55205	0.55097	0.55041	0.54976	0.54911	0.54794
.1500	1.24862	1.24416	1.24157	1.23849	1.23524	1.22936
.2000	2.23626	2.22460	2.21712	2.20681	2.19688	2.18022
.2500	3.52823	3.50389	3.48509	3.46564	3.44544	3.40970
.3000	5.14275	5.09540	5.06532	5.02979	4.99235	4.92473
.3500	7.10415	7.02624	6.97635	6.91611	6.85170	6.73366
.4000	9.44450	9.32203	9.24248	9.14461	8.98563	8.71281
.4500	12.20600	12.01720	11.85480	11.66790	11.40470	11.03870
.5000	15.44440	15.11890	14.89110	14.59560	14.19540	13.36660
.5500	19.23480	18.72250	18.35800	17.88660	17.33220	16.22549
.6000	23.68040	22.87650	22.30840	21.49730	20.47749	20.37900

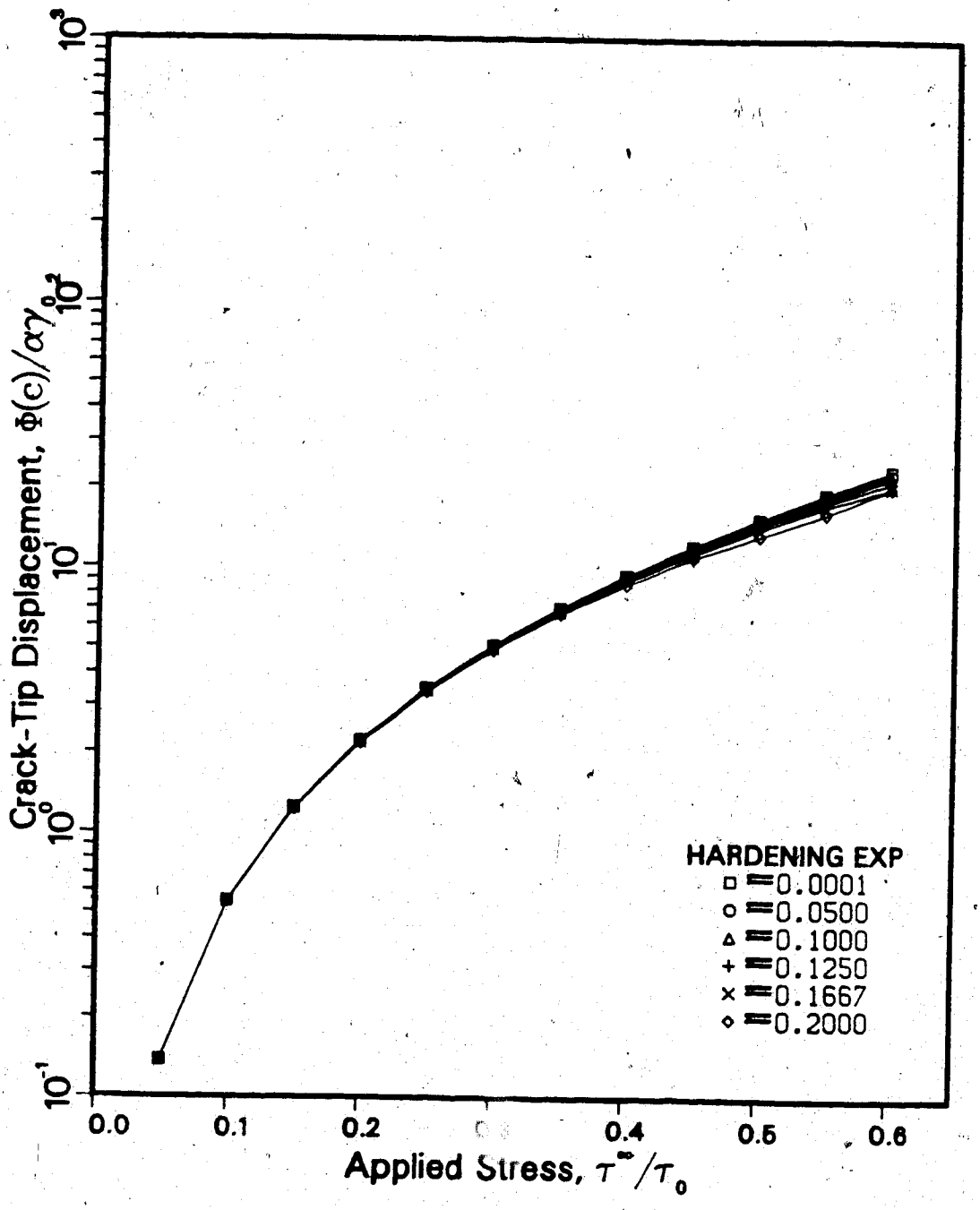

Figure 4.2 The effect of hardening on crack-tip displacement

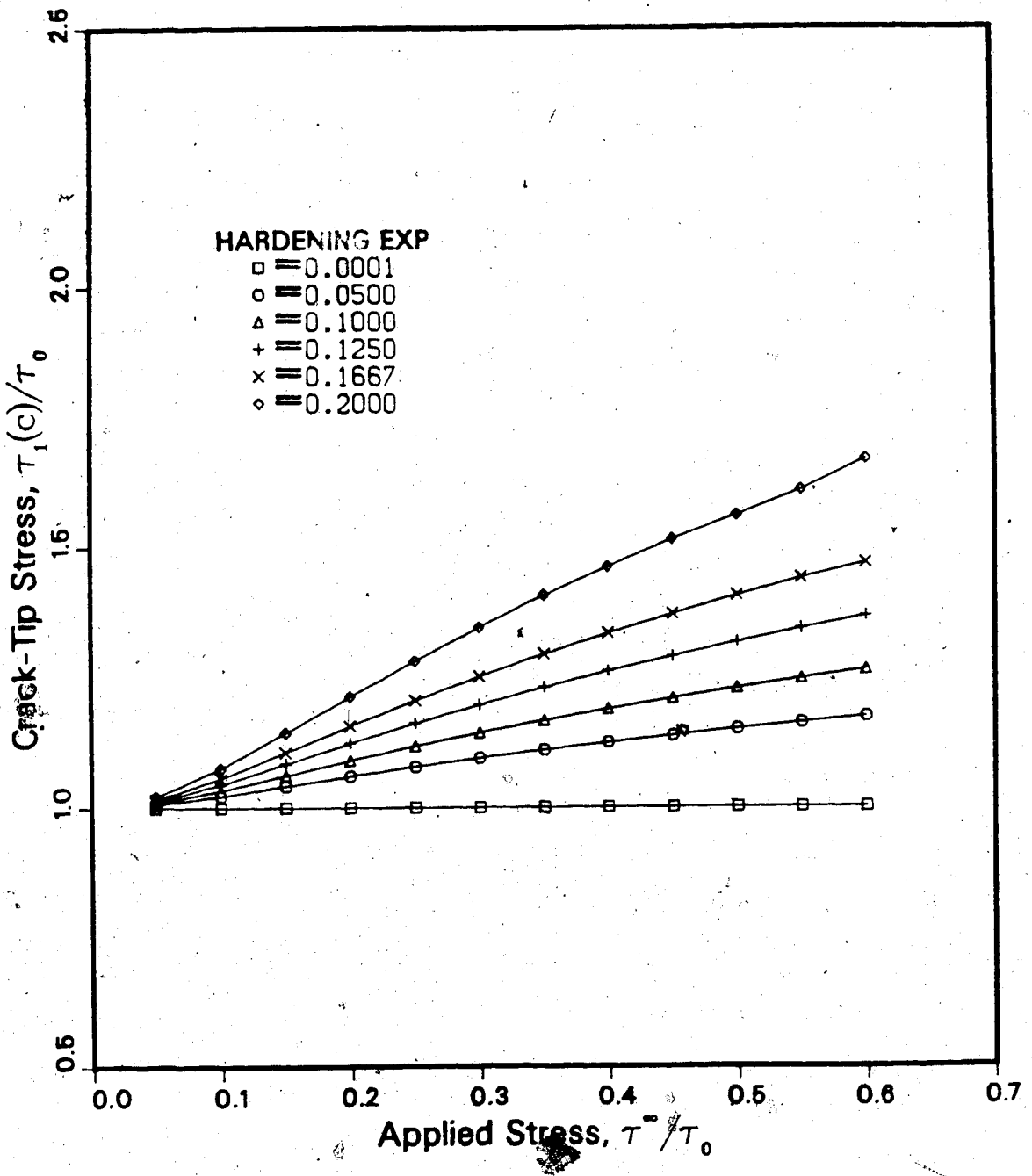

Figure 4.3 The effect of hardening on crack-tip stress

the various values of the hardening exponent. The trend here, as expected, is that the crack-tip stress increases with the applied loading. For a fixed amount of the far-field loading, it is also evident that the crack-tip stress increases with the amount of work-hardening.

Using the crack-tip displacement as a criterion for plastic damage at the crack-tip, the result would indicate that work-hardening reduces the plastic damage. The exactly opposite conclusion might be reached using the crack-tip stress. In Fig. 4.4, another quantity, the strain energy density at the crack-tip, based on both displacement and stresses, is plotted. From this Figure, it is clear that the strain energy density increases with both applied stress and the extent of work-hardening in the material depicted by n'.

In all the quantities considered so far, the value at a given point, (in this case, the crack-tip) was considered. In order to demonstrate the variation in the plastic damage with either applied stress or work-hardening, it is necessary to choose a parameter that is defined for the whole plastic zone. Such a parameter is the J-integral. Earlier investigators have related this to the strain energy density. This can be done here, using Eq. 4.63. In general, there is no closed form solution to the displacement function $\phi(x)$. A numerical integration of Eq. 4.63 enables us to calculate the J-integral for various values of n'. This can also be made dimensionless

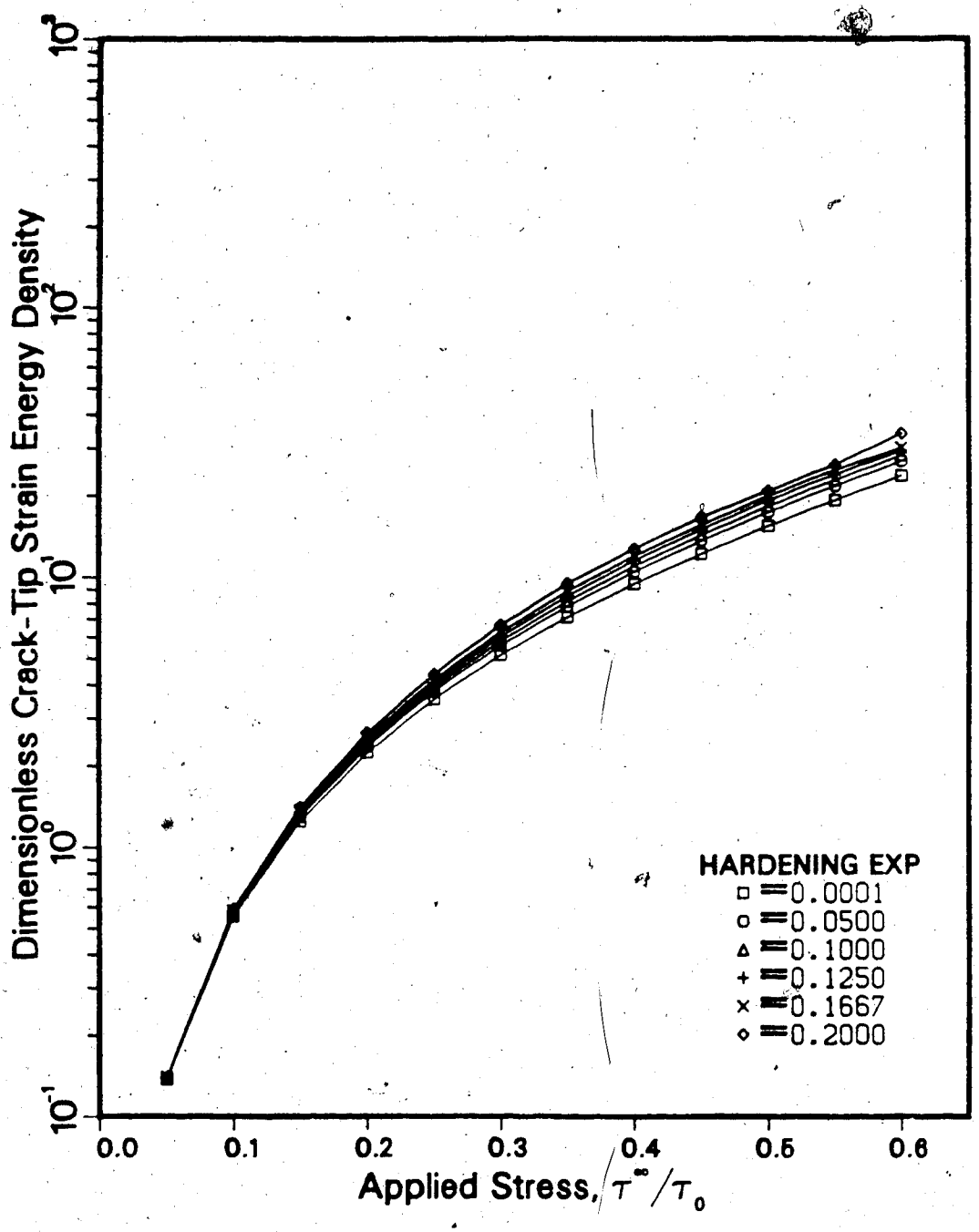

Figure 4.4 The effect of hardening on crack-tip strain energy density

by dividing by the quantity, $\alpha\gamma_o\tau_o$. The dimensionless J-integral is plotted against the applied far field, dimensionless strain energy density as shown in Fig. 4.5. The linearity of the curves shows that there is a power law relationship of the type,

$$J = C(W^{\infty})^{m} \tag{4.64}$$

where C and m are dependent on both the applied loading, and the hardening exponent.

A special case exists in Eq. 4.64. When n'=0, Eq. 4.63 can be integrated analytically. In this case,

$$J = -\tau_o \int_c^a d\,\phi(x) = \tau_o\,\phi(c), \tag{4.65}$$

since $\phi(a)=0$.

Using the vector (1,0,1,0,0,1,0,1) for $\{\alpha_i\}$ in Eq. 4.58,

$$\begin{aligned}\phi(c) &= 2Bc\,\ell n(a/c)\\ &= 2Bc\,\ell n\left\{\sec\frac{\pi\tau^{\infty}}{2\tau_o}\right\}\\ &= 2\,Bc\left[\frac{\pi^2}{8}\left(\frac{\tau^{\infty}}{\tau_o}\right)^2\left\{1-\frac{\pi^2}{16}\left(\frac{\tau^{\infty}}{\tau_o}\right)^2\right\}\right]\end{aligned} \tag{4.66}$$

In the last expression, the first two terms of the

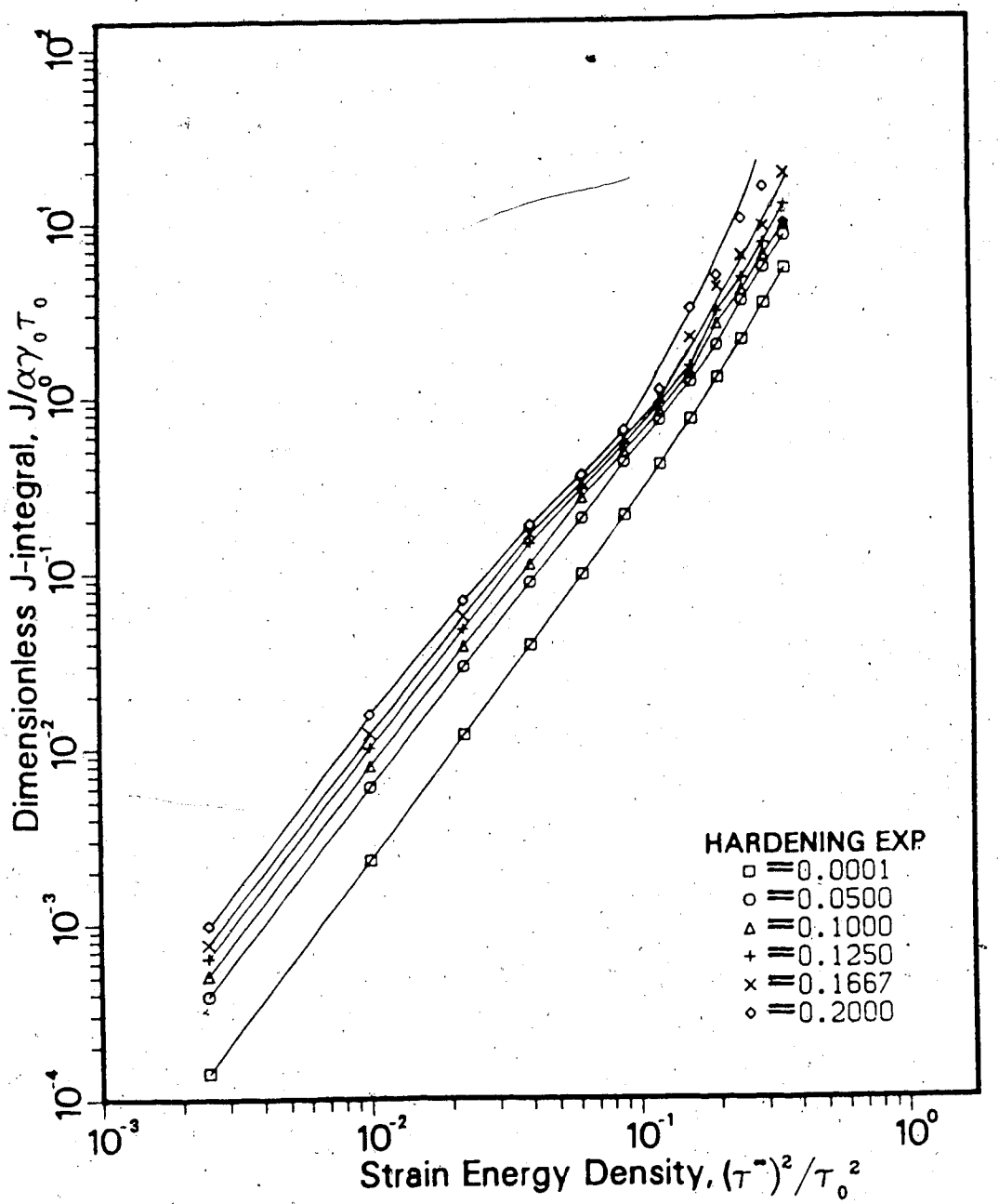

Figure 4.5 The effect of hardening on the J-integral

Taylor's series expansion have been taken.

Substituting Eq. 4.66 in 4.65,

$$J = (1 - \nu)\pi\, c \left[1 - \frac{\pi^2}{16}\left(\frac{\tau^\infty}{\tau_0}\right)^2\right] W^\infty \qquad 4.67$$

where writing $W = (\tau^\infty)^2/2\mu$, is substituted for the far field strain energy density.

Note that, in Eq. 4.67, if $\tau^\infty \ll \tau_0$, i.e., for small scale yielding,

$$J = (1 - \nu)\pi c\, W^\infty \qquad 4.68$$

In which case, J is linearly related to W^∞.

4.7 Comparison With Continuum Models

The original elastic-perfectly plastic model of BCS has been shown to compare favorably with the continuum based model of Hult and McClintock [17,29]. This comparison was made on the basis of the extent of the plastic zone only. Analytical results [19] and, more recently, experimental results [59,60] are available in the literature for comparison with the elastic-nonlinear hardening model presented here. Figures 4.6 to 4.15 are the comparisons of the predicted crack-line strain, stress and Strain Energy Density compared with the continuum model of Rice [19]. As these Figures show, there is considerable disparity between the two predictions in the

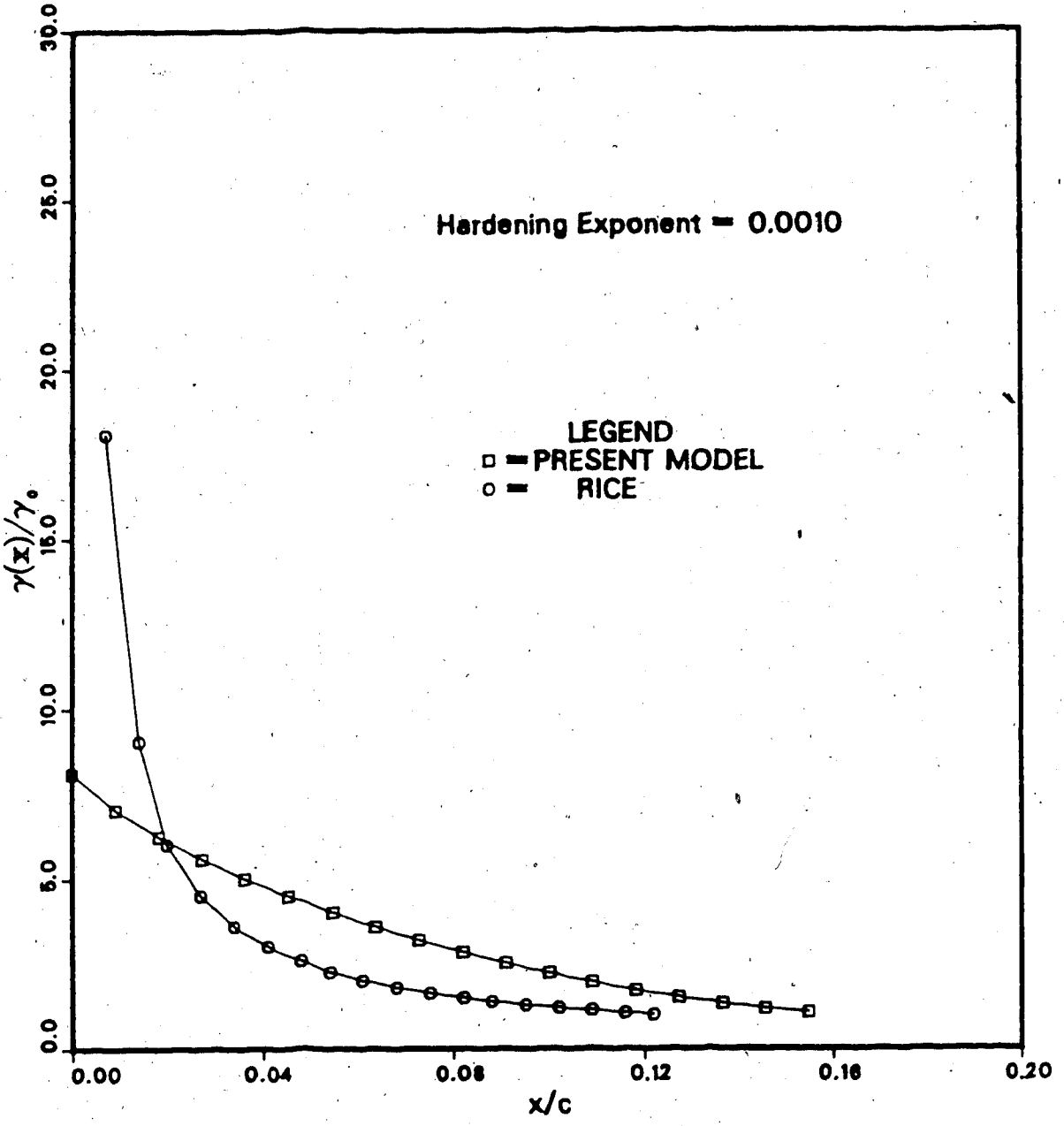

Figure 4.6 Crack-line strain comparison (negligible hardening)

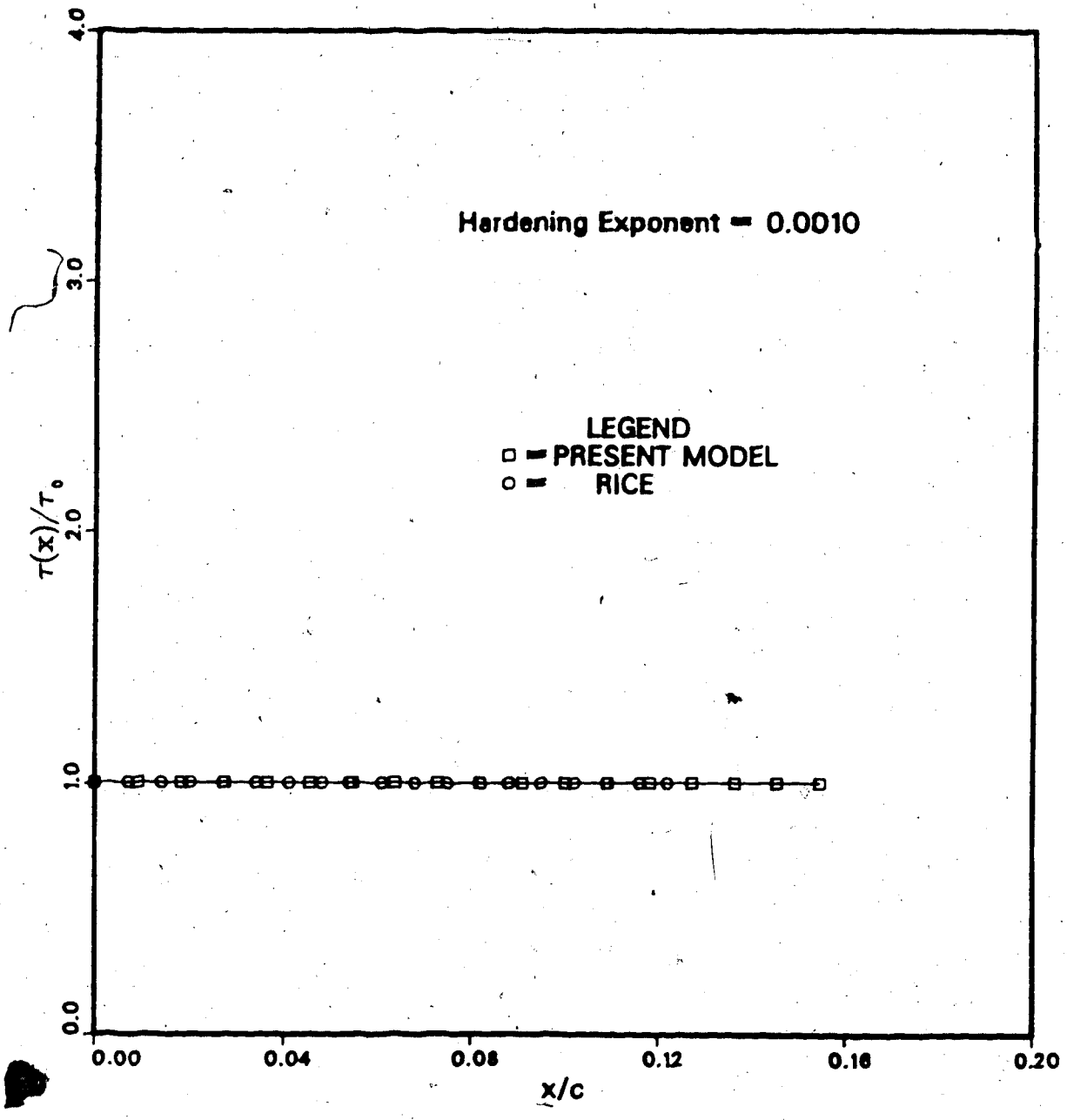

Figure 4.7 Crack-line stress comparison (negligible hardening)

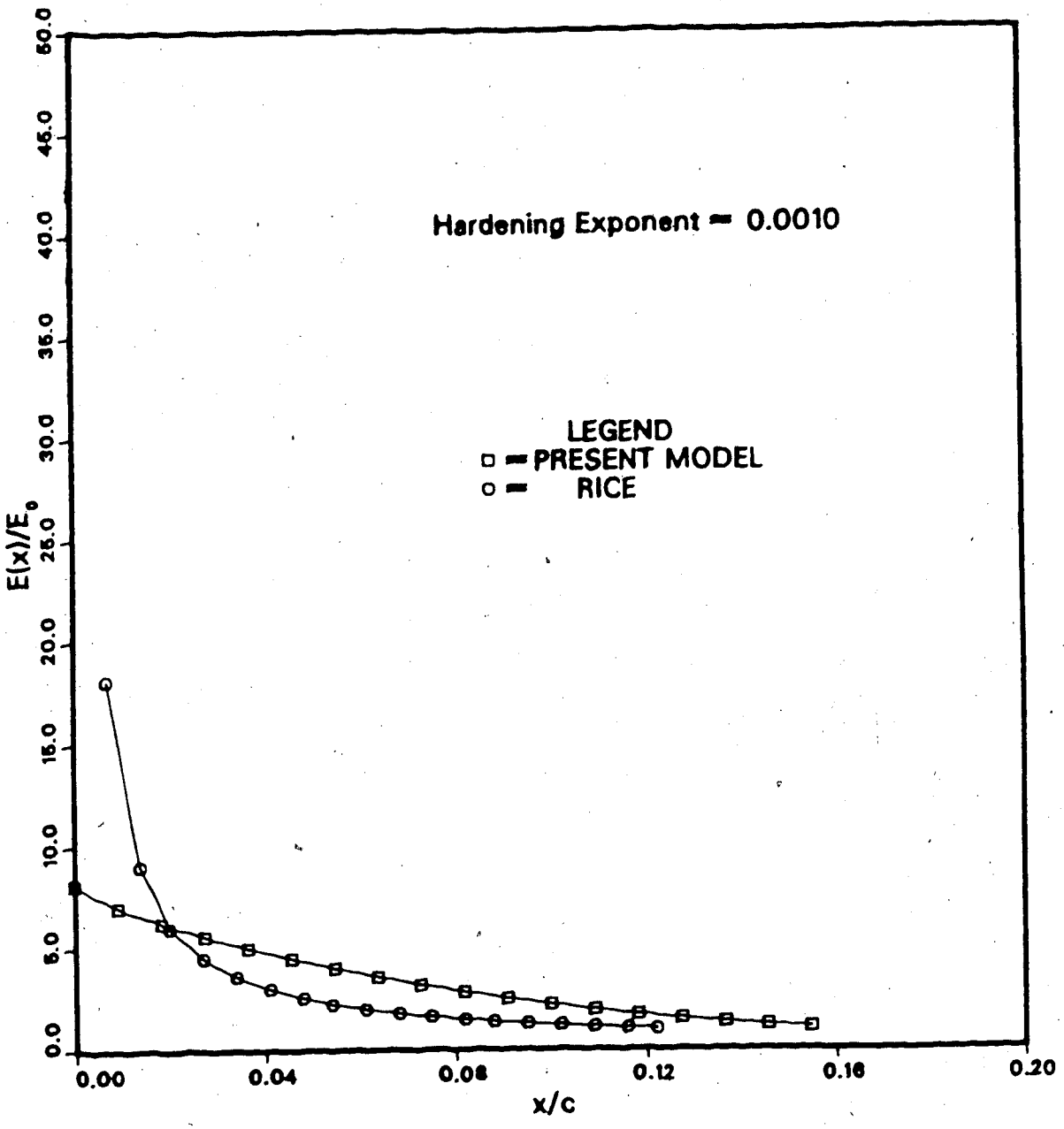

Figure 4.8 Crack-line strain energy density comparison (negligible hardening)

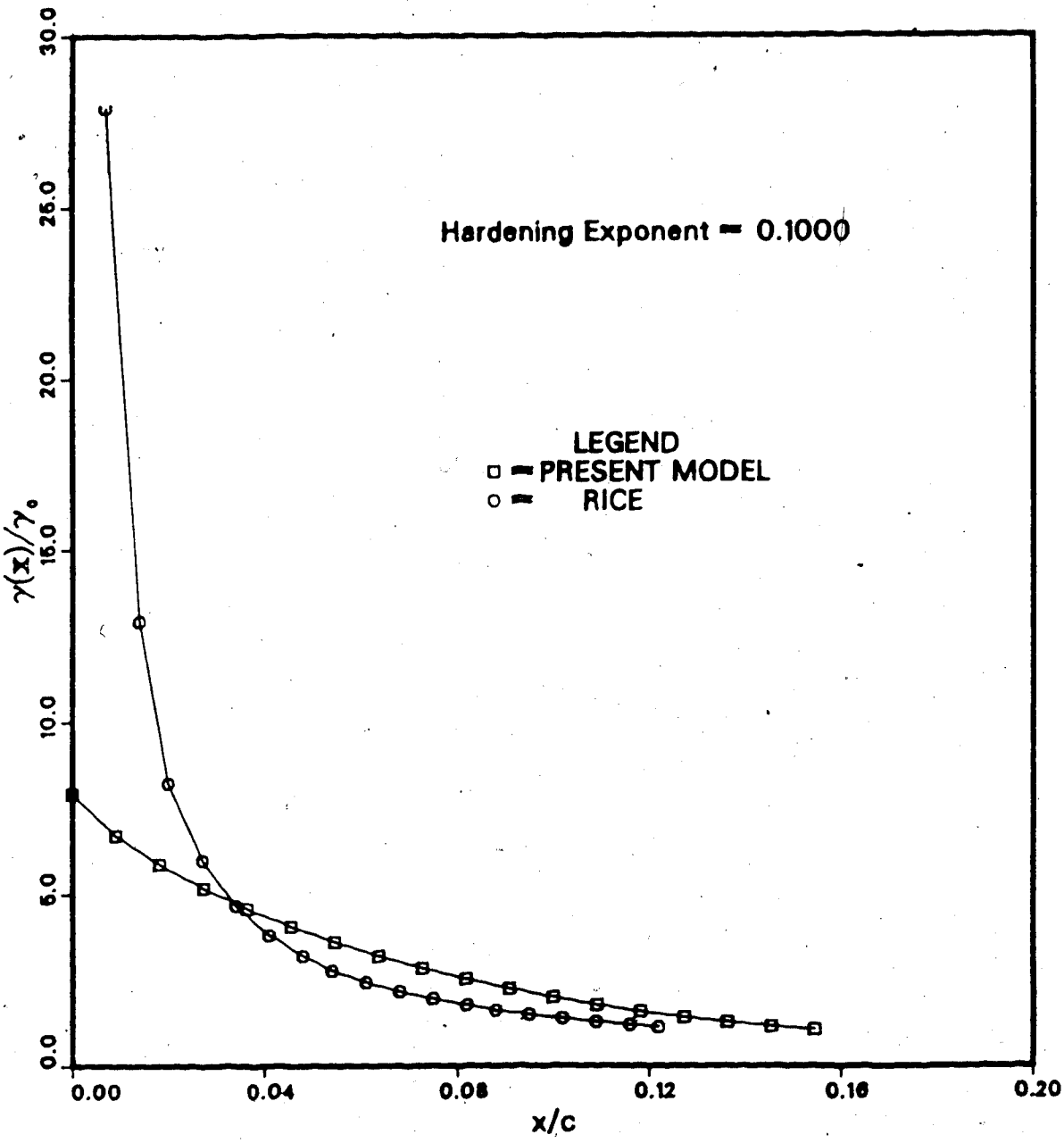

Figure 4.9 Crack-line strain comparison (mild hardening)

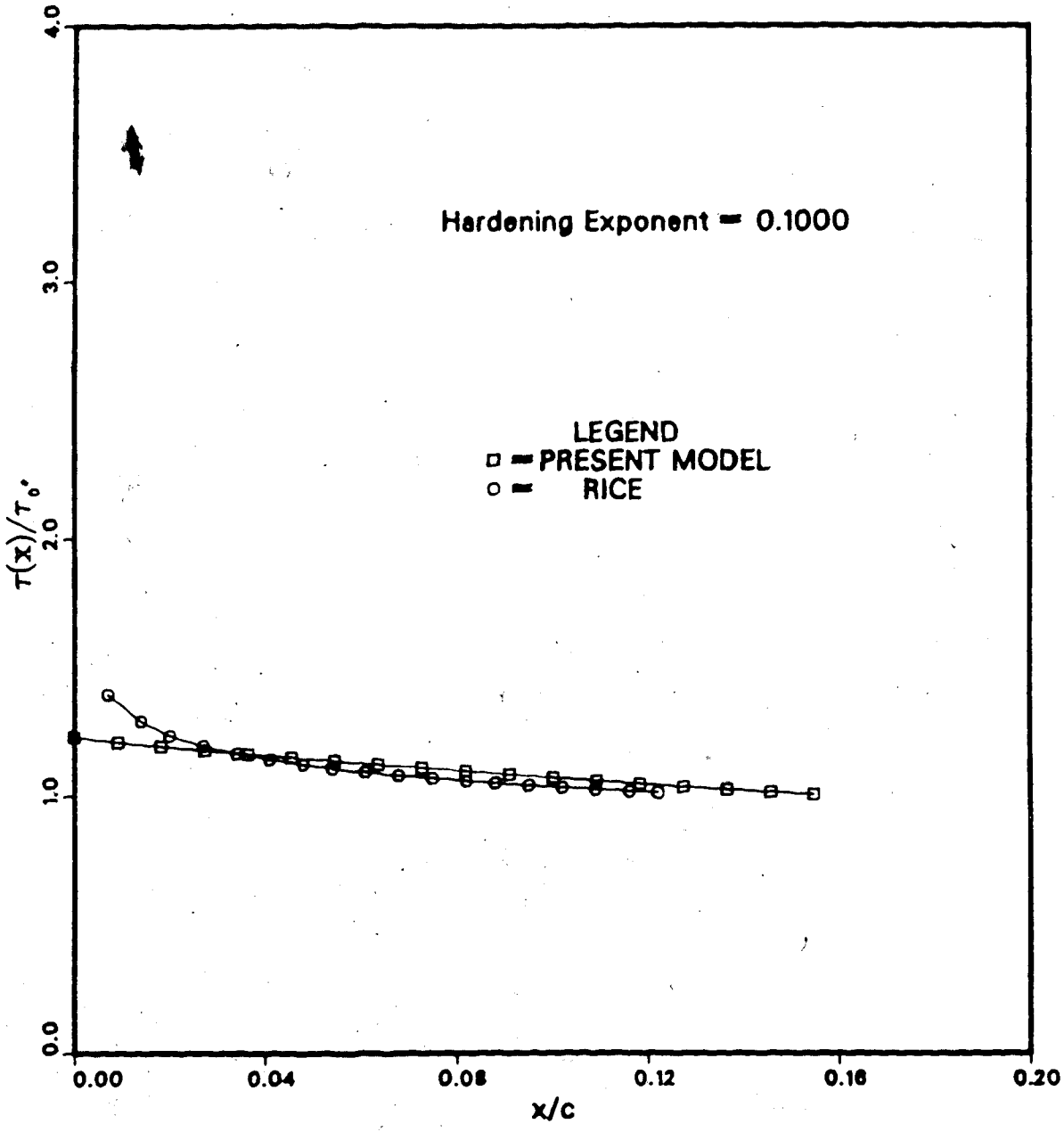

Figure 4.10 Crack-line stress comparison (mild hardening)

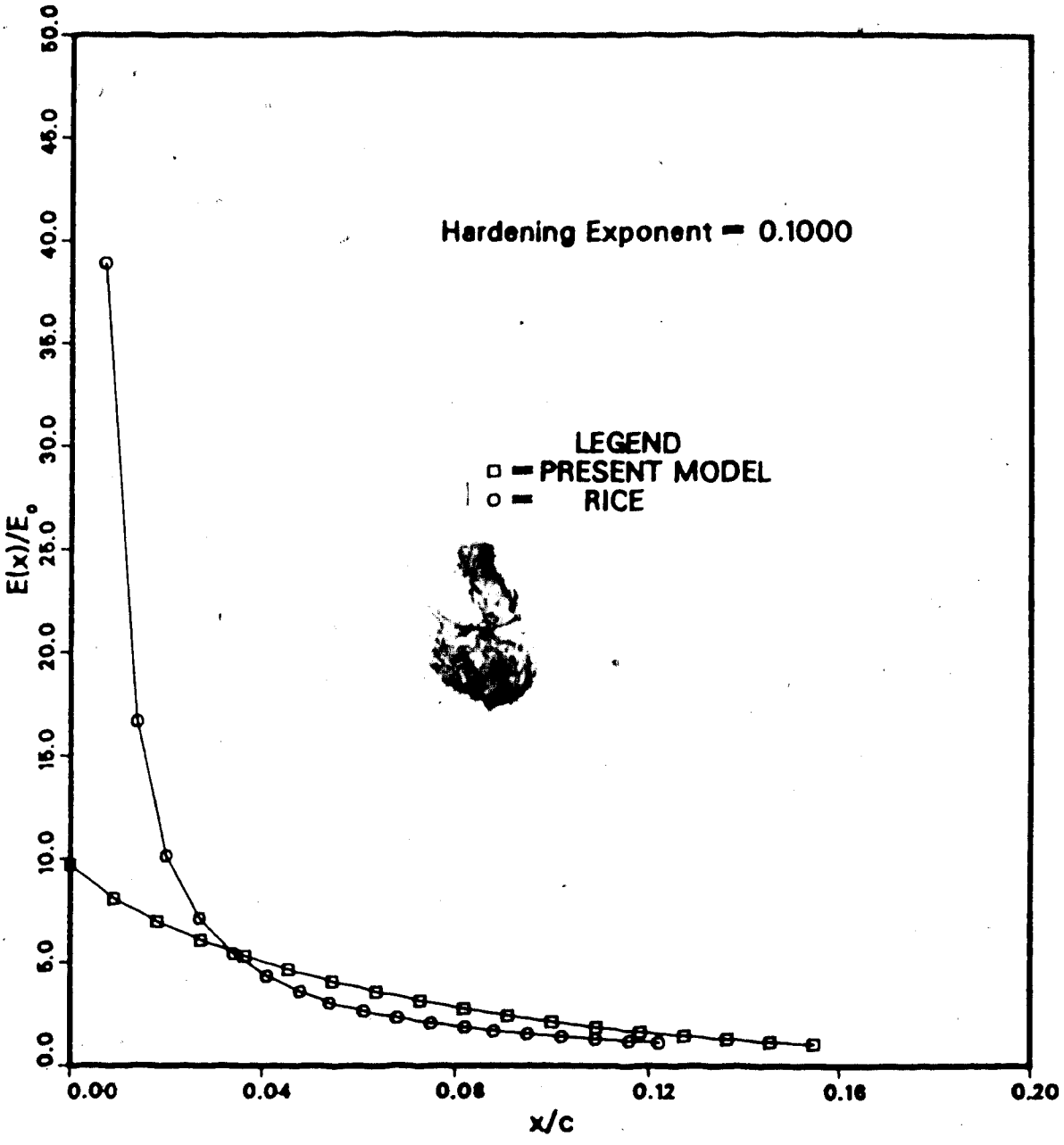

Figure 4.11 Crack-line strain energy density comparison (mild hardening)

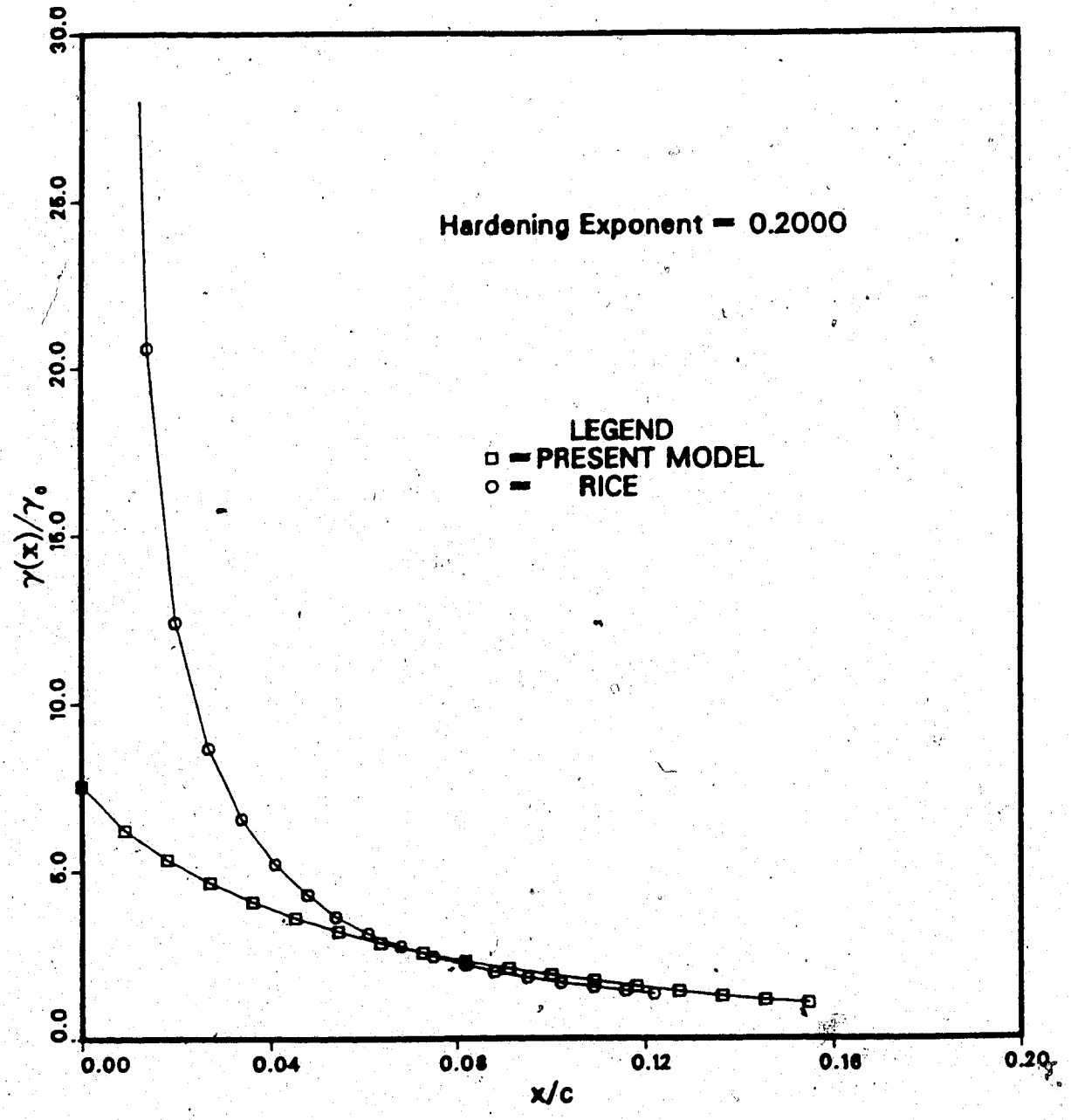

Figure 4.12 Crack-line strain comparison (hign hardening)

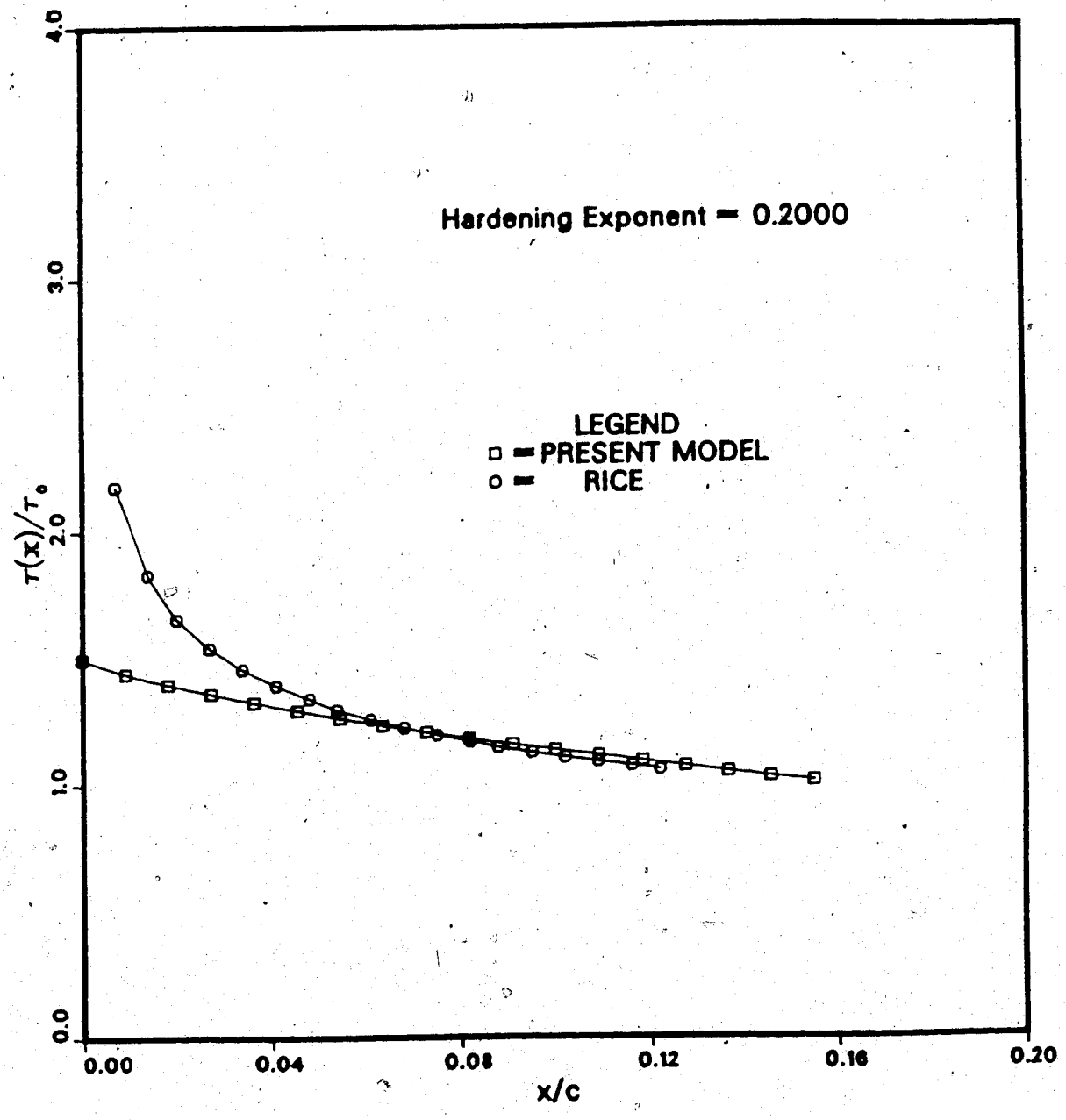

Figure 4.13 Crack-line stress comparison (high hardening)

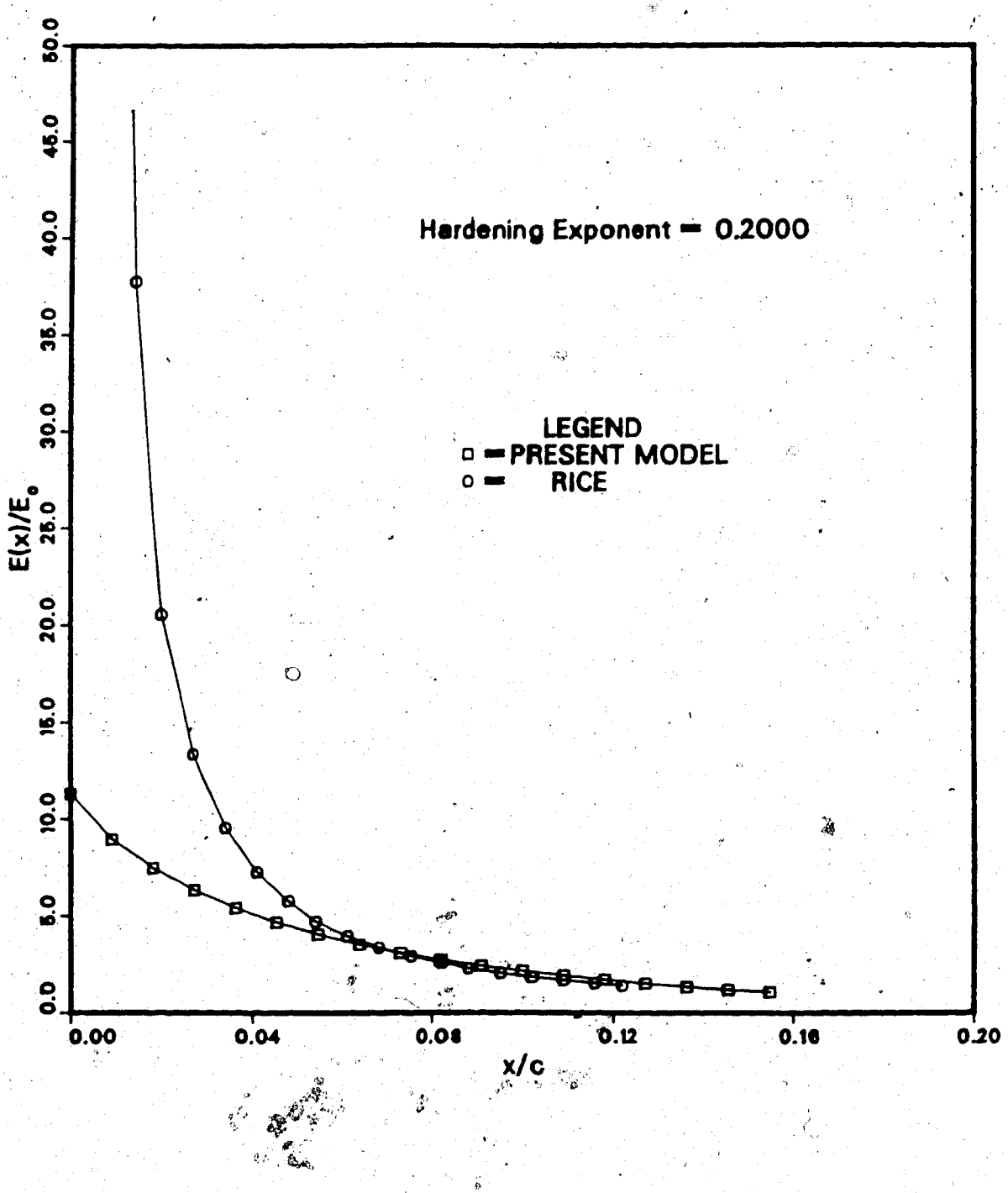

Figure 4.14 Crack-line strain energy density comparison (high hardening)

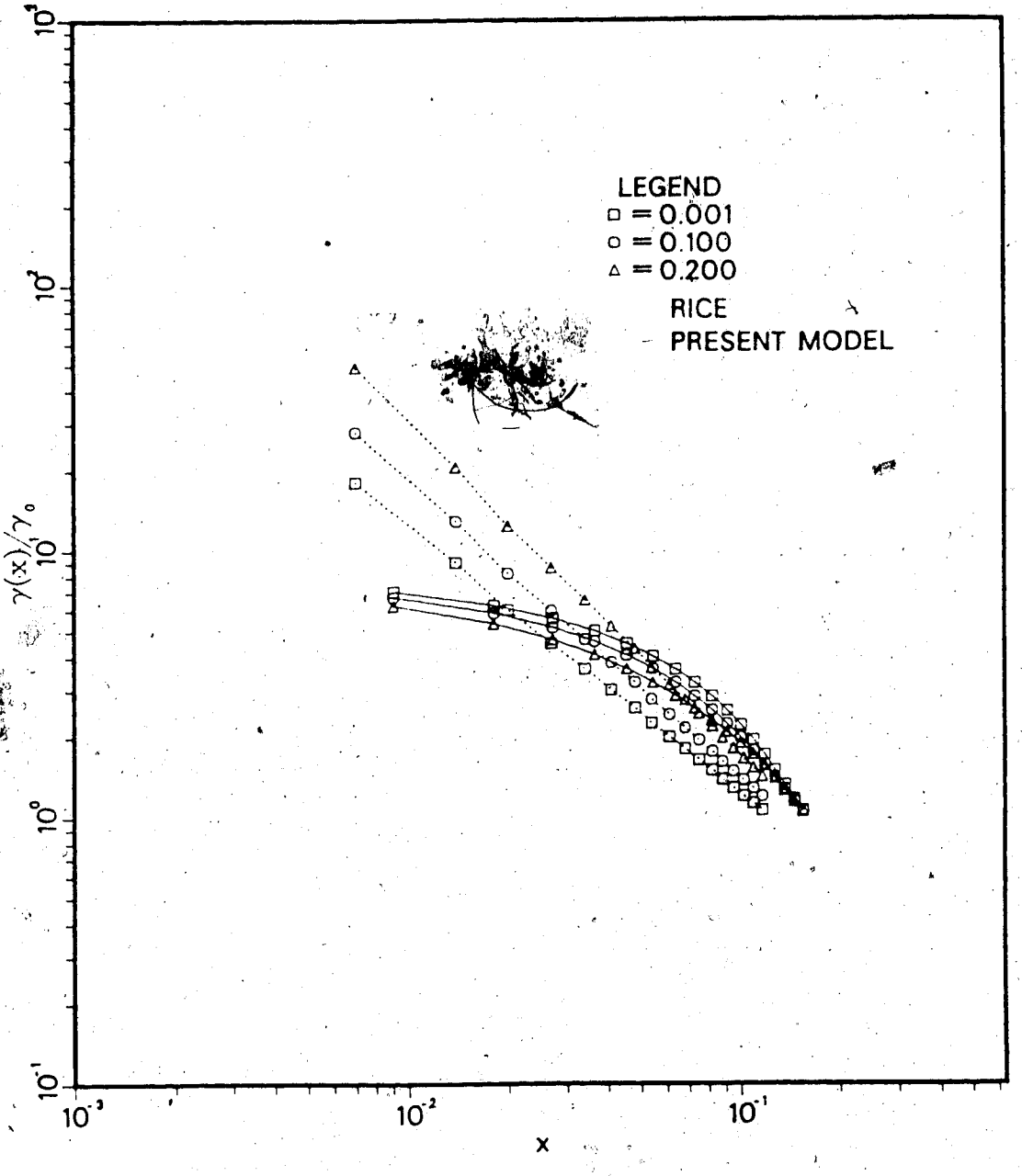

Figure 4.15 Crack-line strain comparison with continuum results on log-log scale

first 15% of the plastic zone size. This results mainly from the singularity predicted by the latter at the crack-tip. This dislocation model predicts finite values of stress/strain at this point for the various values of the hardening exponent. If this first part of the plastic zone is ignored, the prediction the two models are close. Figures 4.6 to 4.8 are for n'=0.001, which is practically elastic-perfectly plastic. The other two sets of figures, 4.9 to 4.11 and 4.12 to 4.14, represent n'=0.1 and 0.2 respectively. These correspond to mild and high hardening cases. It can be seen that the predicted strains in the two models become closer as the hardening exponent increases. The results for the stresses are even better in general. The Strain Energy Density predicted from these two are also close to each other. These two models thus result in similar predictions for the stress/strain field if the first 15% of the plastic zone size is ignored. We shall discuss this disparity region shortly.

It is significant that the predictions at the ends of the plastic zone are very similar in both models despite the fact that there is a significant diference in the plastic zone sizes in the two models. The values of the strain, stress and the strain energy density predicted by the two models are very close to each other.

We now return to the first 15% of the plastic zone size where the two models differ most. Figure 4.15 shows the plot of the strain distribution versus the

crack-tip distance on a log-log scale. As expected, the greatest difference is observed as $x \to 0$. Available experimental results, however, support this model rather than Rice's in this part of the plastic zone. The crescent shape of this dislocation model prediction is exactly the same as has been observed by Davidson and Lankford [59] for various metals with differing hardening exponents. These investigators have shown that the strain distribution at the origin flattens out in the same way as this dislocation model behaves. This also justifies the singularity removal method used in chapter 3 where the stress/strain distribution at the crack-tip neghbourhood was assumed approximately constant.

Chapter 5

UNLOADING FIELD AND CYCLIC J-INTEGRAL

5.1 Introduction

The dislocation model developed in the previous chapter can be applied to the problem of a crack that is first loaded, and then unloaded to a specified value. This can be further applied to the case of the cyclically loaded crack. The application of dislocation to fatigue loading is not entirely new. Weertman [36], and later Lardner [35], have extended the original BCS [17] monotonic loading model to the case of cyclic loading. In these works, attention is restricted to the displacement at the crack-tip. Crack growth either results from the attainment of a critical value of the crack-tip displacement, or in the fatigue cycling case, when the sum of the displacements at the tip attains a critical value.

From the results in chapter 4, it was seen that work-hardening does not change the crack-tip displacement considerably. Since work-hardening usually leads to a reduction in the value of crack-tip displacement, applying the fatigue ductility failure criterion (as in ref. [7] for instance) would lead to a conclusion then that work-hardening should lead to a lower crack growth rate. Stated differently, this means that the plastic damage rate at the crack-tip should be lower, the higher the work-hardening rate in a given material.

It should be noted that these models presume that the crack-tip stress is always at the yield level. As a result of this limitation, it is not possible to obtain a criterion for cyclic crack growth based on crack-tip stress, or any other stress related quantity. Using the results of Chapter 4, we find that if the crack growth theory is based on the attainment of a critical stress value, a higher work-hardening material would lead to higher crack growth, and higher plastic damage rate. This is a diametrically opposite conclusion from the displacement based criterion. It is therefore evident that, neither the crack tip stress, nor the crack-tip displacement is a consistent measure of the crack-tip plastic damage.

It is desirable to have a crack growth criterion that is not restricted to the crack-tip values. A consideration of the entire plastic zone will be necessary to account for the plastic damage ahead of the crack which results in crack propagation. Such a criterion is the cyclic J-integral proposed by Tanaka [39]. Unfortunately, the evaluation of this quantity has been presented using the classical dislocation theory - limited to the elastic perfectly plastic situation where the entire plastic line is assumed to be maintained at the material yield stress. This is therefore again a quantity based on the plastic displacement considerations only, even though in this case attention is no longer restricted to the crack-tip values.

Applying the complete work-hardening dislocation model to the cyclic case will facilitate the evaluation of a cyclic J-integral dependent both on the plastic displacement as well as the stress field ahead of the crack-tip. Using such a quantity as a crack growth criterion, one would expect to avoid the inconsistency already noted in the use of either a displacement or stress based criterion.

In ref. [39] the plastic superposition method of Rice [19] was used to obtain the stress/strain field ahead of an unloaded crack. The dislocation modelling of the unloaded crack here can be viewed as a generalization of Rice's method. Moreover, one major inconsistency of the plastic superposition method is avoided. This inconsistency arises in the fact that the stress-strain relationship in the plastic zone is nonlinear. This implies that the superposed stress obtained from Rice's method is no longer related to a similarly obtained superposed strain through the stress/strain relationship. While the dislocation modelling of the unloading yields identical results with Rice's superposition method, its premises are different, and they can be extended naturally to the case of work-hardening, as we shall do shortly.

5.2 Work Hardening Unloading Problem

(a) Hardening Laws

In the post yield behaviour of any material, the loading funtion, ℓ, defines the yield surfaces beyond the

initial one in the form of:

$$\ell(\sigma_{ij}, \varepsilon^{p}_{ij}, K) = 0 \qquad 5.1$$

where, σ_{ij} are the stress components, ε^{p}_{ij} are the plastic strain components, and, K represents the way work-hardening enters the loading function.

Equation 5.1 is a general equation defining the changes in the yield surface as a result of the strain hardening. It is the manner in which ε^{p}_{ij} enters the equation that is of concern here. For the purpose of explaining the work-hardening dislocation model of unloading, it is sufficient to consider the one dimensional case here. This is depicted in Fig. 5.1.

After an initial loading to the yield point, (or surface), depicted as τ_0, continued loading leads to plastic strain $\gamma_p(x)$. This leads to the creation of a subsequent yield point at stress equal to $\tau_1(x)$. The difference between the initial yield point and the final yield point is τ_p. When the material is unloaded as shown, the incipience of the plastic strain depends on the hardening law. It is generally accepted that, due to Bauschinger effects, plasticity would begin earlier than the value of the negative initial yield stress, $-\tau_0$. It is convenient to represent this reduction in the negative yield point in terms of τ_p. Clearly, from the Figure, the value $\beta = 0$ represents a situation where there is no

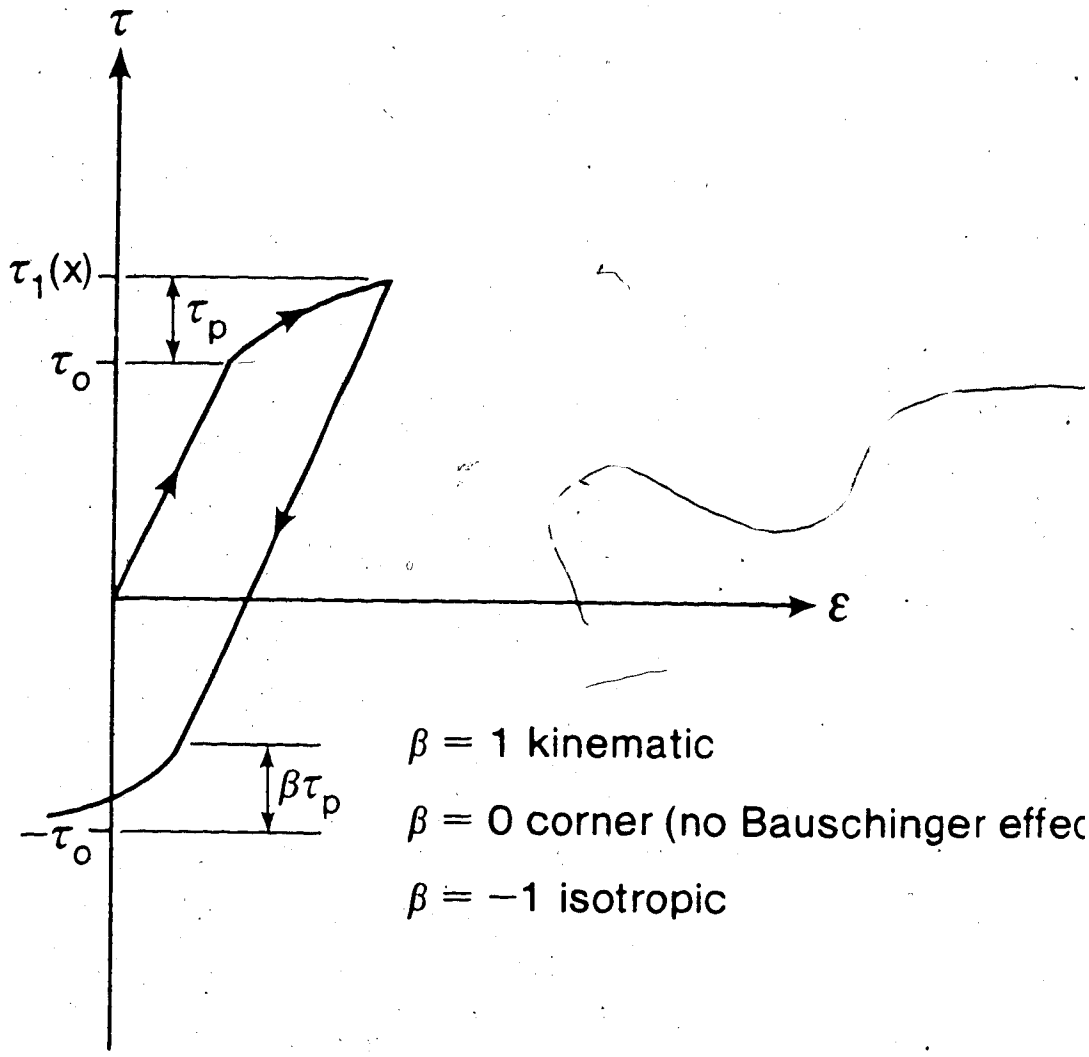

Figure 5.1 Reversed yield point for various hardening rules - one dimensional case

Bauschinger effect, in which case the yield surface is "anchored" at the stress level of $-\tau_0$. This is also called "CORNER HARDENING". The two simplest cases considered in the literature are, $\beta = \pm 1$, called kinematic and isotropic hardening respectively. In the former case, the yield surface is merely translated without any distortion (at least in the direction of loading), while the second case corresponds to a uniform expansion in the axis under consideration. In general, the hardening law is such that the yield surface is both translated and distorted. In this study, attention is restricted to the situation where $|\beta| \leq 1$.

(b) The Unloading Problem

For a work-hardening material loaded to a specified level of stress as described in chapter 4, consider a reduction in the applied stress of magnitude . The non-equilibrium created by this reduction leads to reversed forces on the dislocations along the plastic line. The friction stress at each point will then be adjusted in magnitude and direction to oppose dislocation motion. In some locations, near the crack-tip, the reversed forces will be sufficient to move some of the dislocations back into the crack-tip reducing the dislocation density (just as an increase in the applied stress would have led to a dislocation density increase). For the positions closer to the end of the plastic line, $x = \pm a$, the reversed forces may not be sufficient to cause reversed motion. For all

such locations, the dislocations already embedded during the loading are "locked" into their positions until the applied loading is sufficiently high to overcome the initial friction stresses present. Therefore, there is a reduction in the dislocation density from the crack-tip to a point "δ" (Fig. 5.2), while the density function between δ and a remains unchanged. Since the change in the plastic displacement is caused by the amount of reduction in the dislocation density, the functional form of the friction stress is assumed unchanged from Eq. 4.6, i.e.

$$\tau_{11}(x) = F(\Delta\phi(x)) - \beta\, \tau_p(x) \qquad 5.2$$

where $\Delta\phi(x)$ = the change in the plastic displacement due to the unloading at point x, $\tau_p(x) = \tau_1(x) - \tau_0$ and, $-1 < \beta < 1$.

The last term on the RHS of Eq. 5.2 is necessary to account for the displacement and the translation of the initial yield surface at each point due to the work-hardening. This is illustrated in Fig. 5.1. Since τ_0 is interpreted as the yield stress, $\beta\tau_p$ is the amount by which the initial yield stress is reduced in the reversed loading, to account for the Bauschinger effect. It is to be noted that β accounts for both translation and distortion of the yield surface in the one dimensional case. Let g(x) be the resultant dislocation density in the equilibrium state reached after the unloading. Provided

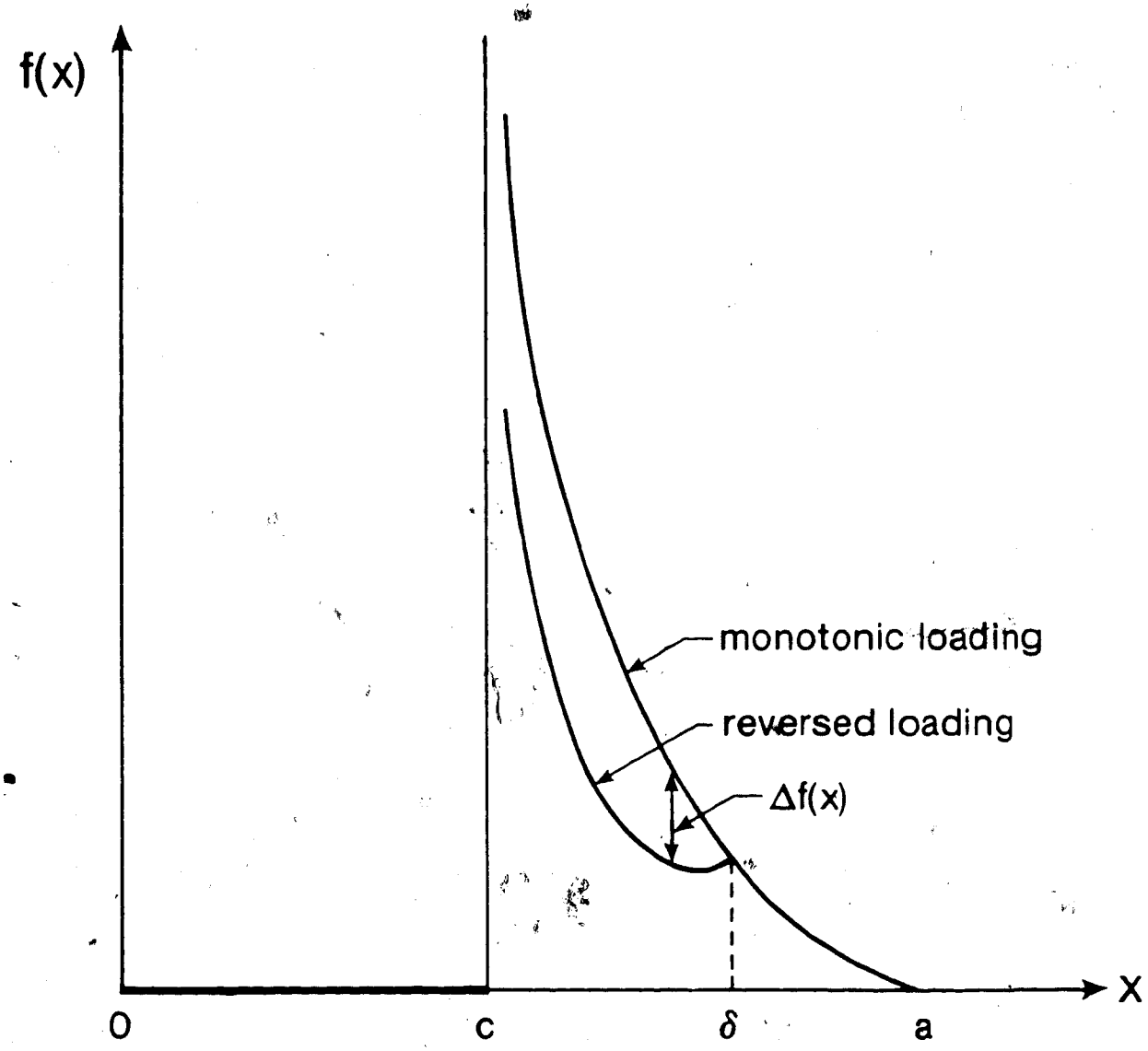

Figure 5.2 Loading and unloading dislocation density functions

$\delta < a$, application of equilibrium equation to the unloaded crack implies:

$$\int_{-a}^{a} \frac{g(x')dx'}{x-x'} + \frac{Q(x)}{A} = 0 \qquad 5.3$$

where

$$Q(x) = \begin{cases} \tau^{\infty} - \tau & |x| < c \\ \tau^{\infty} - \tau - \tau_{11}(x) & c < |x| < \delta \\ \text{unknown} & \delta < |x| < a \end{cases} \qquad 5.4$$

It has been assumed here that there is no contact between the two crack surfaces, so that only the effect of the far field loading contributes the non-dislocation forces at each point in the range $|x| < c$. The resistance of the friction stress in $\delta < |x| < a$ will vary from a value $\tau_{11}(x)$, opposing motion, to a value of $\tau_1(x)$, opposing the original motion of the dislocation, hence supporting the motion in the reversed direction. In this region therefore,

$$\tau^{\infty} - \tau - \tau_1(x) < Q(x) < \tau^{\infty} - \tau + \tau_{11}(x) \qquad 5.5$$

Subtracting equation 5.3 from 4.7, one gets,

$$\int_{-\delta}^{\delta} \frac{f(x')-g(x')}{x-x'} + \frac{H(x)}{A} = 0 \qquad 5.6$$

where
$$H(x) = \begin{cases} \tau & |x| < c \\ \tau - \tau_1(x) - \tau_{11}(x) & c < |x| < \delta \end{cases}$$

$$= \begin{cases} \tau & \\ \tau - 2\tau_0 & \end{cases} - \begin{cases} 0 & \\ (1-\beta)\{F(\phi(x)) - \tau_0\} & \end{cases} - \begin{cases} 0 & |x| < c \\ \text{[illegible]}(x)) - \tau_0 & c < |x| < \delta \end{cases}$$

$$H(x) = H_1(x) - H_2(x) - H_3(x) .$$

Using $H_1(x)$ instead of $H(x)$, Eq. 5.6 becomes the elastic-perfectly plastic unloading equilibrium equation, derived by Lardner [35].

The inversion of 5.6 follows the same pattern as already described in section 4.3. Substituting $f(x') - g(x')$ for $f(x')$ and $H(x)$ for $D(x)$ in Eq. 4.45, assuming that $f(x') - g(x')$ belongs to the class H^*, and $H(x)$ belongs to the class H, then,

$$f(x) - g(x) = \frac{2(1-\nu)}{\pi\mu b} \int_{-\delta}^{\delta} R_1(x, y)\, H(y)\, dy \qquad 5.7$$

where
$$R_1(x,y) = \frac{1}{x - y} \sqrt{\left\{\frac{\delta^2 - x^2}{\delta^2 - y^2}\right\}}$$

The change in the plastic displacement due to the

unloading can then be derived,

$$\Delta\phi(x) = \int_{-\delta}^{\delta} b\{f(x') - g(x')\}dx'$$

$$= \Delta\phi_0(x) - B(1-\beta)\int_{c}^{\delta}\{(\frac{\phi(y)}{\alpha\gamma_0} + 1)^{n'} - 1\}K_1(x,y)dy$$

$$- B\int_{c}^{\delta}\{(\frac{\Delta\phi(y)}{\alpha\gamma_0} + 1)^{n'} - 1\}K_1(x,y)dy, \qquad 5.8$$

where $$\Delta\phi_0(x) = \int_{x}^{\delta}\frac{b}{\pi^2 A}\int_{-\delta}^{\delta} R_1(x';y)H_1(x')dx'dy$$

is the elastic-perfectly plastic unloading displacement distributions [35],

$$R_1(x,y) = \frac{1}{x-y}\sqrt{\frac{\delta^2-x^2}{\delta^2-y^2}},$$

$$K_1(x,y) = \int_{x}^{\delta}\{R_1(x';y) + R_1(x';-y)\}dx \qquad 5.9$$

and

$$\frac{1}{2B}\Delta\phi_0(x) = (x+c)\cosh^{-1}\left|\frac{\delta^2-x^2}{\delta(x+c)} + \frac{x}{\delta}\right|$$

$$- (x-c)\cosh^{-1}\left|\frac{\delta^2-x^2}{\delta(c-x)} + \frac{x}{\delta}\right|$$

The second term on the RHS of equation 5.8 contains $\phi(x)$, the plastic displacement at each position at maximum loading, while the last term contains $\Delta\phi(x)$, the change in plastic displacement at each position. Therefore, it follows that the change in plastic displacement is dependent on both the range of unloading, as well as the amount of the maximum loading in the range. Other parameters affecting the change in plastic displacement are, of course, the hardening exponent n', and the "cyclic hardening factor", β. Setting n'=0, equation 5.8 becomes identical to the elastic-perfectly plastic solution of Lardner [35], irrespective of the value of the parameter β. This is to be expected because the term containing β cannot take any other value than zero when n'=0. In order to see this, consider the fact that this non work-hardening case corresponds to a retention of the original yield surface, so that there is no reduction of the yield stress in the unloading situation, therefore $\tau_p(x)$, defined in Fig. 5.1, is equal to zero.

It is necessary that the change in the dislocation density be bounded at the points $\pm\delta$. The conditions for this to be the case can be derived in a similar way as in equation 4.35. If H(x) in 5.6 is substituted for F(x) in 4.35, one obtains, after some rearrangements,

$$\int_{-c}^{c} \frac{\tau dx}{(\delta^2 - x^2)^{\frac{1}{2}}} + \left(\int_{-\delta}^{-c} + \int_{c}^{\delta} \right) \frac{\tau - \tau_I(x) - \tau_{II}(x)}{(\delta^2 - x^2)^{\frac{1}{2}}} dx = D \qquad 5.10$$

This is the cyclic equivalent of the boundedness condition in Eq. 4.35.

5.3 Solution of the Unloading Displacement Equations

The two unknown quantities in equations 5.8 and 5.10 are the change in plastic displacement, $\Delta\phi(x)$, and the extent of the cyclic plastic zone δ. The integral equation 5.8, and the boundary condition, 5.10 can be solved simultaneously for these two quantities as outlined in section 4.4. The expansion method, used in the latter was also employed with two main modifications. Firstly, it was found that the change in the monotonic plastic zone (compared to the perfectly plastic case) was insignificant. Hence, the elastic-perfectly plastic zone size was used in this analysis. This can be obtained from 5.10 by setting n'=0;

$$\int_{-c}^{c} \frac{\tau dx}{(\delta^2 - x^2)^{\frac{1}{2}}} + \left(\int_{-\delta}^{-c} + \int_{c}^{\delta} \right) \frac{\tau - 2\tau_0}{(\delta^2 - x^2)^{\frac{1}{2}}} dx = Q \qquad 5.11$$

which means, $c/\delta = \cos(\pi\tau/4\tau_0)$.

This approximation leads to a great simplification of the computational procedure, and, judging from the results

obtained in section 4.4, the reduction in accuracy is minimal. Secondly, analogous to the procedure in chapter 4, the unknown change in plastic displacement was approximated by a perturbation of the elastic-perfectly plastic unloading fuction (Eq. (5.1)),

$$\frac{1}{2B}\Delta\phi(x) = \alpha_1(x+c)\cosh^{-1}\left[(1+|\alpha_2|)\left|\frac{\delta^2-c^2}{\delta(c+x)}+\frac{c}{\delta}\right|\right.$$

$$\left.-\alpha_3(x-c)\cosh^{-1}\left[(1+|\alpha_4|)\left|\frac{\delta^2-c^2}{\delta(c-x)}+\frac{c}{\delta}\right|\right]\right. \qquad 5.12$$

where the exponential-Gaussian background in Eq. 4.58, has been removed. This was done because there was little change to the initial parameter input for both the exponential and the Gaussian terms in the monotonic solution.

Apart from these two modifications, the solution method here is as described earlier, so no further details are given. Various values of the hardening exponents as well as values of the parameter β, depicting the cyclic hardening rule, were considered in the ranges, $0 < n' < 0.2$, and $-1 < \beta < +1$. For an initial maximum loading of $0.4\tau_o$, the values of unloading in the range $0.0\tau_o \leq \Delta\tau \leq 0.6\tau_o$ were considered. This was used to study the effect of hardening on the unloading displacement distribution as well as other relevant crack-tip

parameters. In order to study the effect of the mean applied stress in the range, the value of unloading was fixed (here at 0.35 τ_o), and various mean applied stresses were chosen.

The convergence characteristics of the unloading problem was found to be similar to the monotonic loading problem considered in chapter 4. The convergence was faster for lower values of applied unloading, and lower values of the work-hardening exponent n'. The reverse was the case when the applied unloading was higher.

5.4 The Unloading J-Integral

Consider the loading sequence depicted in Fig. 5.3. For any two loading states i → j, following Tanaka [39] the J-integral can be defined as:

$$\Delta J_{j/i} = \int_{\Gamma} (\Delta W dy - \Delta T_m \frac{\partial \Delta u_m}{\partial x} ds) \qquad 5.13$$

where Γ is a suitable integration path around the crack-tip plastic zone.

$\Delta W = \int_{(\varepsilon_{k\ell})_i}^{(\varepsilon_{k\ell})_j} \left(\sigma_{k\ell} - (\sigma_{k\ell})_i \right) d\varepsilon_{k\ell}$ = change in the strain energy density, and,

$\Delta T_m = (T_m)_j - (T_m)_i$ is the change in the traction vector, while, $\varepsilon_{k\ell}$ and $\sigma_{k\ell}$ are the strain and stress tensors

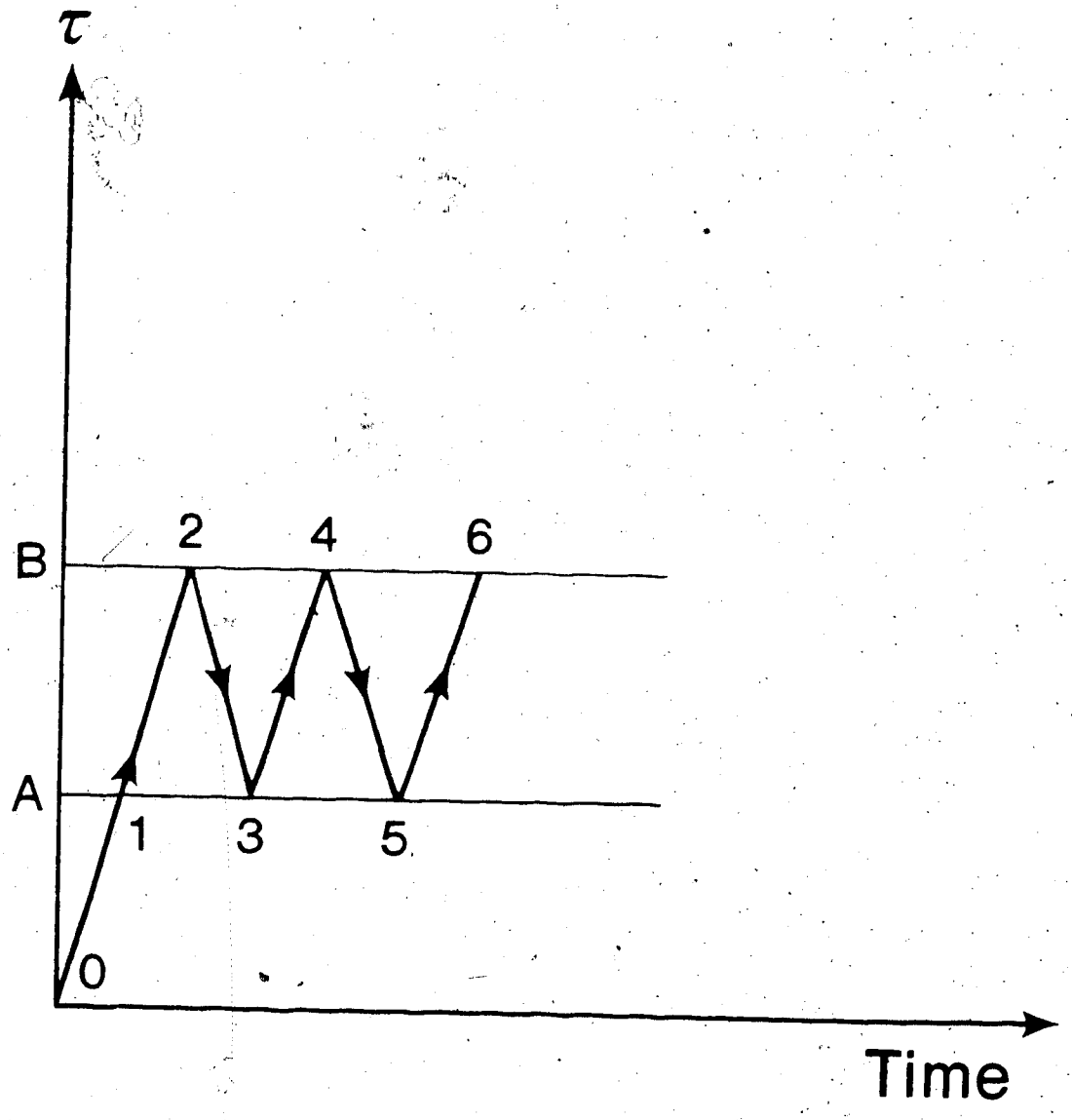

Figure 5.3 Loading sequence

respectively; and $\Delta u_m = (u_m)_j - (u_m)_i$ is the change in the displacement vector. Equation 5.13 has been shown (see appendix) to be path independent just like Rice's J-integral.

Let us consider for the meantime the unloading from 2 → 3. For the plastic line of the dislocation model, taking Γ as the upper and lower surfaces of the plastic zone implies that $dy = 0$. Hence the first term in Eq. 5.13 vanishes, and $ds = dx$.

On the plastic line,

$$\Delta T_m = (T_m)_2 - (T_m)_1 = \tau_{11}(x) - \tau_1(x)$$

which, using 4.6 and 5.2 becomes

$$\tau = \tau_0 \left(\frac{\epsilon(x)}{\alpha\epsilon_0} + 1\right)^{n'} + (1 - \beta)\left(\frac{\epsilon(x)}{\alpha\epsilon_0} + 1\right)^{n'} + \beta \qquad 5.14$$

and,

$$\Delta u_m = \Delta\zeta(x) = b\int_{\zeta}^{\zeta} [f_3(x') - f_2(x')]dx' \qquad 5.15$$

where $f_2(x)$ and $f_3(x)$ are the respective dislocation densities at the states 2 and 3, so that,

$$\Delta J_{3/2} = -\int_{c}^{\delta} \tau_0 \{(\frac{\Delta\phi(x)}{\alpha\gamma_0} + 1)^{n'} + (1-\beta)(\frac{\phi(x)}{\alpha\gamma_0} + 1)^{n'} + \beta\}\frac{\partial\Delta\phi(x)}{\partial x}\, dx \qquad 5.16$$

Equation 5.16 can be evaluated when the parameters (a_1, a_2, a_3, a_4) have been supplied from the least squares optimization solution of equation 5.8 using the function $\Delta\phi(x)$ defined in 5.12, and $\phi(x)$ from 4.58.

For a given level of the initial loading, state 2, (Fig. 5.3) Eq. 5.16 can be used in evaluating the unloading J-integrals for various amounts of unloading, $\Delta\tau$, values of n', and of the parameter β. The effects of the unloading and hardening on the J-integral to mean loading can also be quantified by fixing the amount of unloading stress, $\Delta\tau$ while evaluating $\Delta J_{j/i}$ for various values of initial loading (state 2).

5.5 Results and Discussion

(a) Relationship between unloading and cyclic J-integrals

The procedure outlined in the the last section shows how the unloading J-integral is obtained. It is important to see how this is related to the cyclic J-integral. Figure 5.4 depicts the changes in the dislocation density for the loading sequence in Fig 5.3. The functions $f_1(x)$ and $f_2(x)$ the dislocation densities for states 1 and 2 are of the same shape, and can both be evaluated from the monotonic dislocation solution, Eq. 4.45. The density

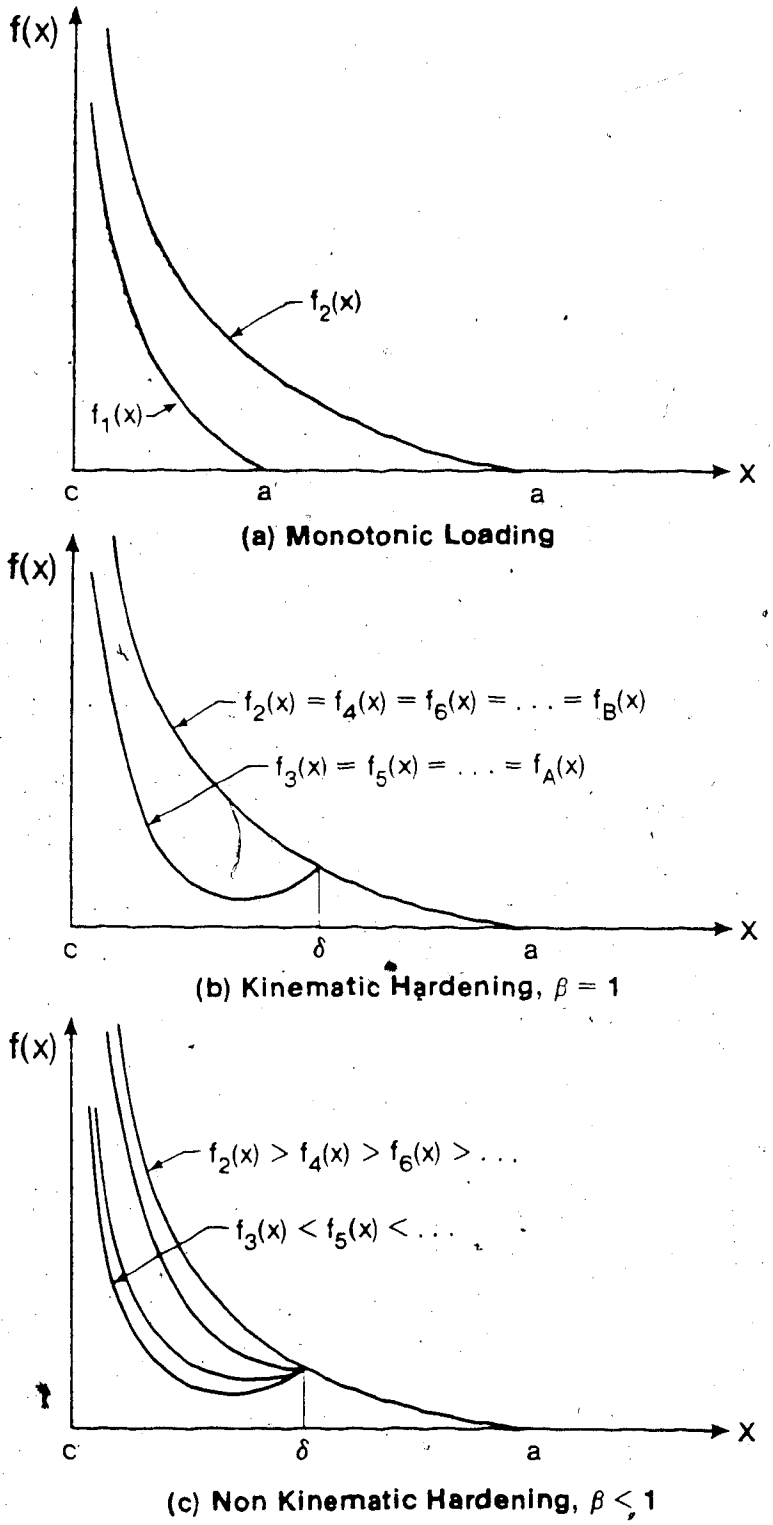

Figure 5.4 Variation of dislocation density with monotonic and cyclic loading

function after the unloading to state 3, is as depicted in Fig. 5.4b. If the τ in equation 5.4 is replaced by the unloading stress range $\Delta\tau$, then, $f_3(x) = g(x)$ in Eq. 5.8. In the reversed plasticity portion (i.e. where some of the dislocations return to the crack-tip, causing a negative change in plastic displacement due to the unloading), there is a reduction in the dislocation density. Outside this region, the unloading is elastic and there is no reversed plasticity. By reloading to state 4, the new dislocation density will depend on the magnitude of the friction stress opposing the return of the dislocations. If the friction stress is the same in state 4 as in state 2 (as in the case of kinematic hardening, $\beta = 1$) the dislocation density would return to its former value at state 2, so that in the sequence we can have $f_2(x) = f_4(x) = f_6(x)$...etc. In this case, $\Delta J_{3/2}$ obtained from Eq. 5.13 is the unique value that quantifies the J-integral in the loading range τ_A and τ_B. In other cases (non-kinematic hardening, $|\beta| < 1$), the friction stress in state 4 will be greater than that in state 2. Unloading to state 5 would also lead to a reversed friction stress of greater amount than before. The resulting dislocation density will be depicted in Fig. 5.4c. $\Delta J_{3/2}$ does not uniquely quantify the J-integral for the range of loading in this case. Its value is the J-integral at the maximum plastic displacement range. This is a reference cyclic J-integral for the loading range in this particular cyclic

hardening law.

(b) Non-Work Hardening Case

In Ref. [5] the cyclic J-integral was expressed as a linear combination of the elastic and plastic strain energy density range. Similar results follow in the dislocation model in the case of constant friction stress provided the applied stress range is small enough. This is shown below.

The relevant cyclic J-integral is obtained from Eq. 5.16 by setting n' = 0, so that,

$$\Delta J_{3/2} = - \int_{c}^{\delta} 2\tau_0 \frac{\partial[\Delta\phi(x)]}{\partial x} dx \, . \qquad 5.17$$

A closed form solution exists for the displacement range function $\Delta\phi(x)$ in this case. It is the same as Eq. 5.12 with $\alpha_1 = 1$, $\alpha_2 = 0$, $\alpha_3 = 1$ and $\alpha_4 = 0$. Since $\Delta\phi(x)$ depends on x alone, from Eq. 5.17, we get

$$\begin{aligned} \Delta J_{3/2} &= 2\tau_0 \{\Delta\phi(c) - \Delta\phi(\delta)\} \\ &= 2\tau_0 \, \Delta\phi(c) \, , \end{aligned} \qquad 5.18$$

as $\Delta\phi(\delta) = 0$. But for the elastic-perfectly-plastic case, from 5.11,

$$\frac{c}{\delta} = \cos\left(\frac{\pi(\Delta\tau)}{4\tau_0}\right) \qquad 5.19$$

Using the values of the α_i's already specified in 5.17,

$$\Delta\phi(c) = 4Bc \log\left(\frac{\delta}{c}\right) , \qquad 5.20$$

And, now, a substitution from 5.19 in 5.20 leads to,

$$\Delta\phi(c) = 4Bc \log\left[1 + \frac{\pi^2}{32}\left(\frac{\Delta\tau}{\tau_0}\right)^2\right]$$

$$= 4Bc\left[\frac{\pi^2}{32}\left(\frac{\Delta\tau}{\tau_0}\right)^2 \{1 - \frac{\pi^2}{64}\left(\frac{\Delta\tau}{\tau_0}\right)^2\}\right] \qquad 5.21$$

where we have ignored all terms expcept the first two in a Taylor's series expansion of the logarithmic and secant functions. The relevant J-integral in this range can be written as,

$$\Delta J_{3/2} = \pi(\Delta W)c \qquad 5.22$$

where $\Delta W = (\Delta\tau/2\mu)^2$ is the far field strain energy density, c is half crack length, and

$$\eta = (1-\nu)\pi \left(1 - \frac{\pi^2}{64}\left(\frac{\Delta\tau}{\tau_0}\right)^2\right) \qquad 5.23$$

It follows therefore, that, provided $\Delta\tau << \tau_0$, η is practically constant, so that, the cyclic J-integral is proportional to the far field strain enery density range.

(c) Effect of Hardening

In the calculations presented, typical alloy steel properties used are μ = 400GPa, τ_0 = 200MPa, and ν = 0.3. Figure 5.5 is a plot of the cyclic J-integral against the far field applied strain energy density on a log-log scale. For moderate levels of the applied stress range, $\Delta\tau$, (keeping the maximum nominal stress at $0.4\tau_0$) the curves are approximately linear for β in the range $-1 < \beta < 1$. Only the two extreme cases (β=±1) are shown here (as in other places in this chapter) for clarity. The approximate linearity on a log-log scale in this case obviously shows that the relationship between ΔJ and the far field strain energy density range is, in general, of a power law type. For each cyclic hardening law (that is, the value of β), the effect of work hardening is quite significant. The magnitude of ΔJ varies by a factor of up to 5 as n' varies from 0.0 to 0.2. For β = 1 (kinematic hardening) the curves are approximately parallel. For a power law relationship of the type,

$$\Delta J = a(\Delta W)^b, \qquad 5.24$$

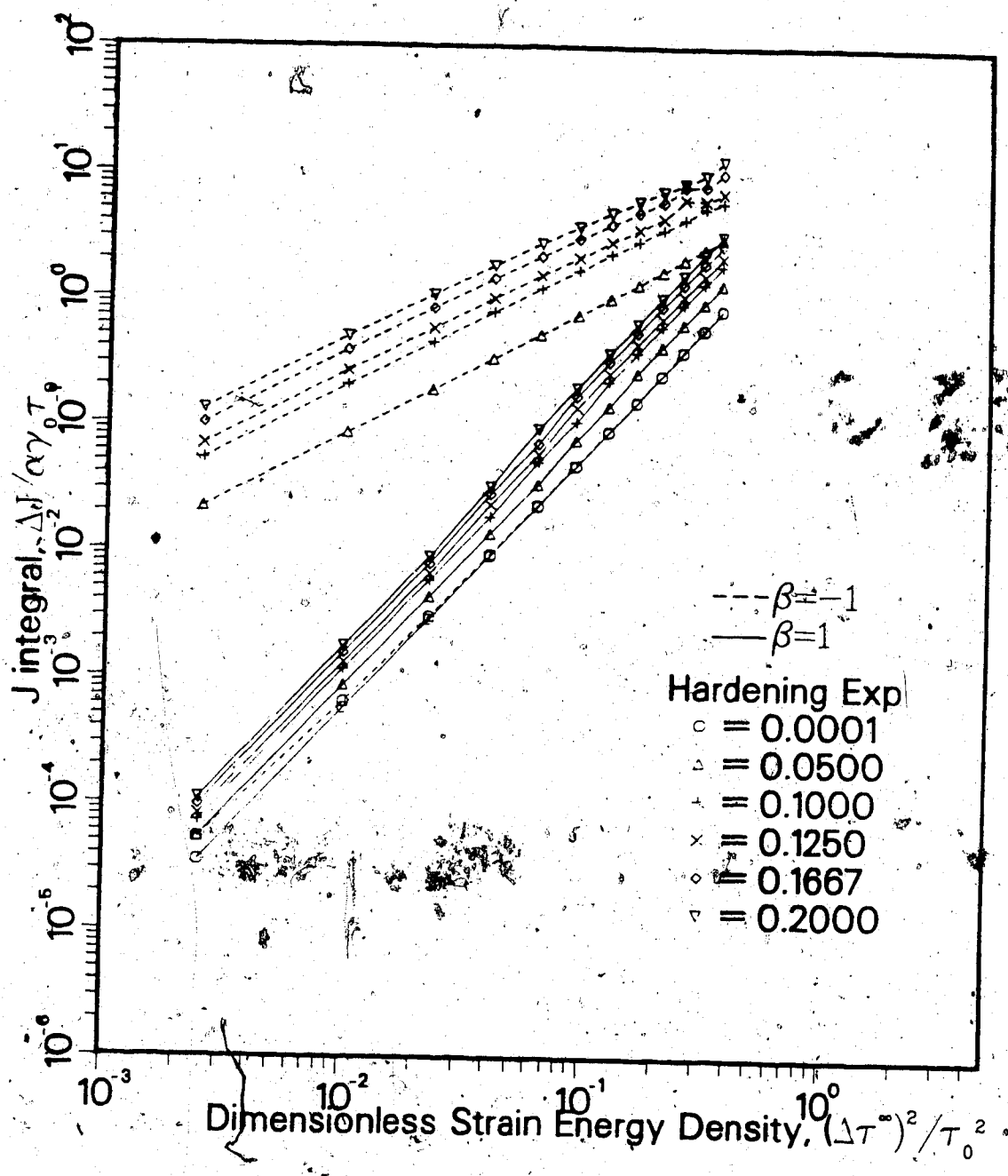

Figure 5.5 Cyclic J-integral vs applied strain energy density

the parameter b is quite insensitive to work-hardening in this case. Most of the work hardening influence is carried through the coefficient parameter a. This is not the case in the non-kinematic work-hardening cases, represented by isotropic hardening $\beta = -1$. These curves change both in slope and intercept as the hardening exponent varies.

Figure 5.6 is the plot of the cyclic crack-tip strain energy density, SED, versus the applied far field stress range. In all cases, the SED increases with applied stress as well as the hardening exponent. The apparent contradiction in the use of either stress or strain to characterise the plastic damage (see section 4.5) can be avoided by basing the cyclic damage on the SED.

In the next set of Figures, the applied stress range is kept fixed at the value of $\Delta\tau = 0.35\tau_o$, while the mean applied stress was allowed to vary between $0.05\tau_o$ and $0.3\tau_o$. In this case, a mean stress value of 0.175 corresponds to the case of complete unloading, $\tau_{min}/\tau_{max} = 0$. In Fig. 5.7, the crack-tip displacement was plotted against the mean applied stress, $(\tau_{max} + \tau_{min})/2\tau_o$. In general, as expected, the crack-tip displacement range decreases with the hardening exponent. This variation is more pronounced in the isotopic hardening case. The exact opposite behaviour is observed when the crack-tip stress is plotted against the mean applied stress (Fig. 5.8). When these two quantities are combined to form the crack-tip SED, Fig. 5.9, it turns out that the latter increases with

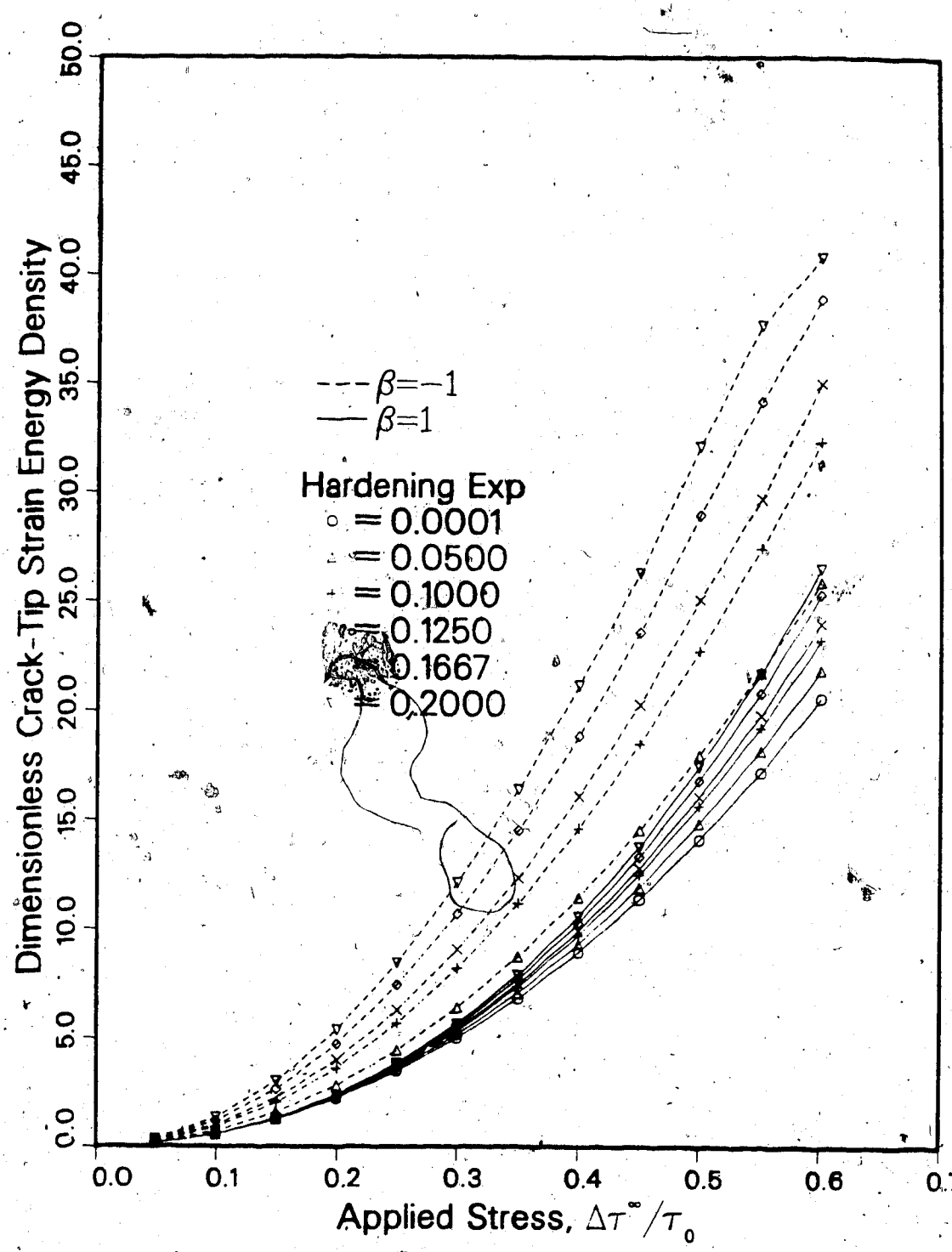

Figure 5.6 Effect of hardening on the crack-tip strain energy density

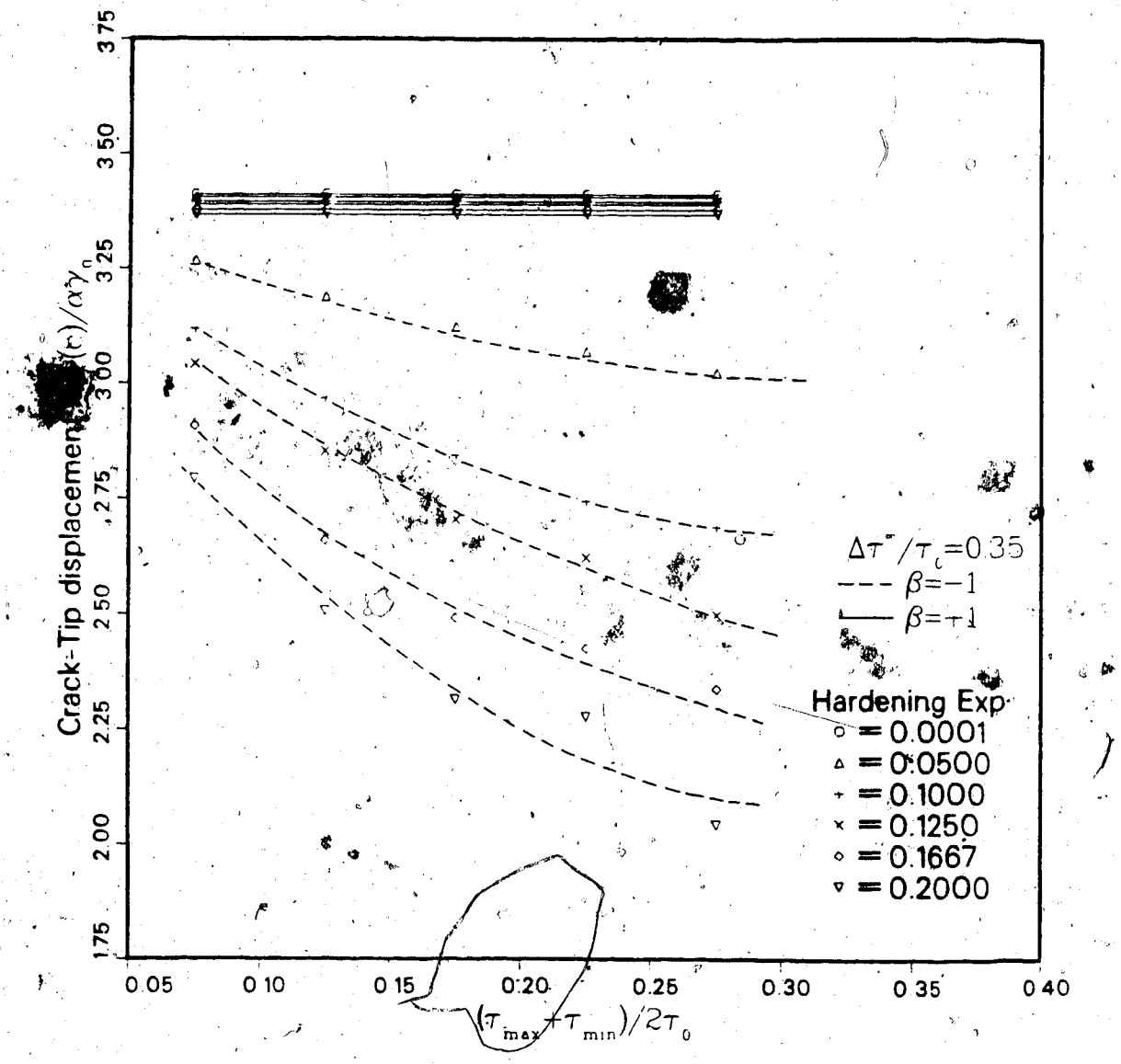

Figure 5.7 Variation of crack-tip displacement range with hardening and mean applied stress

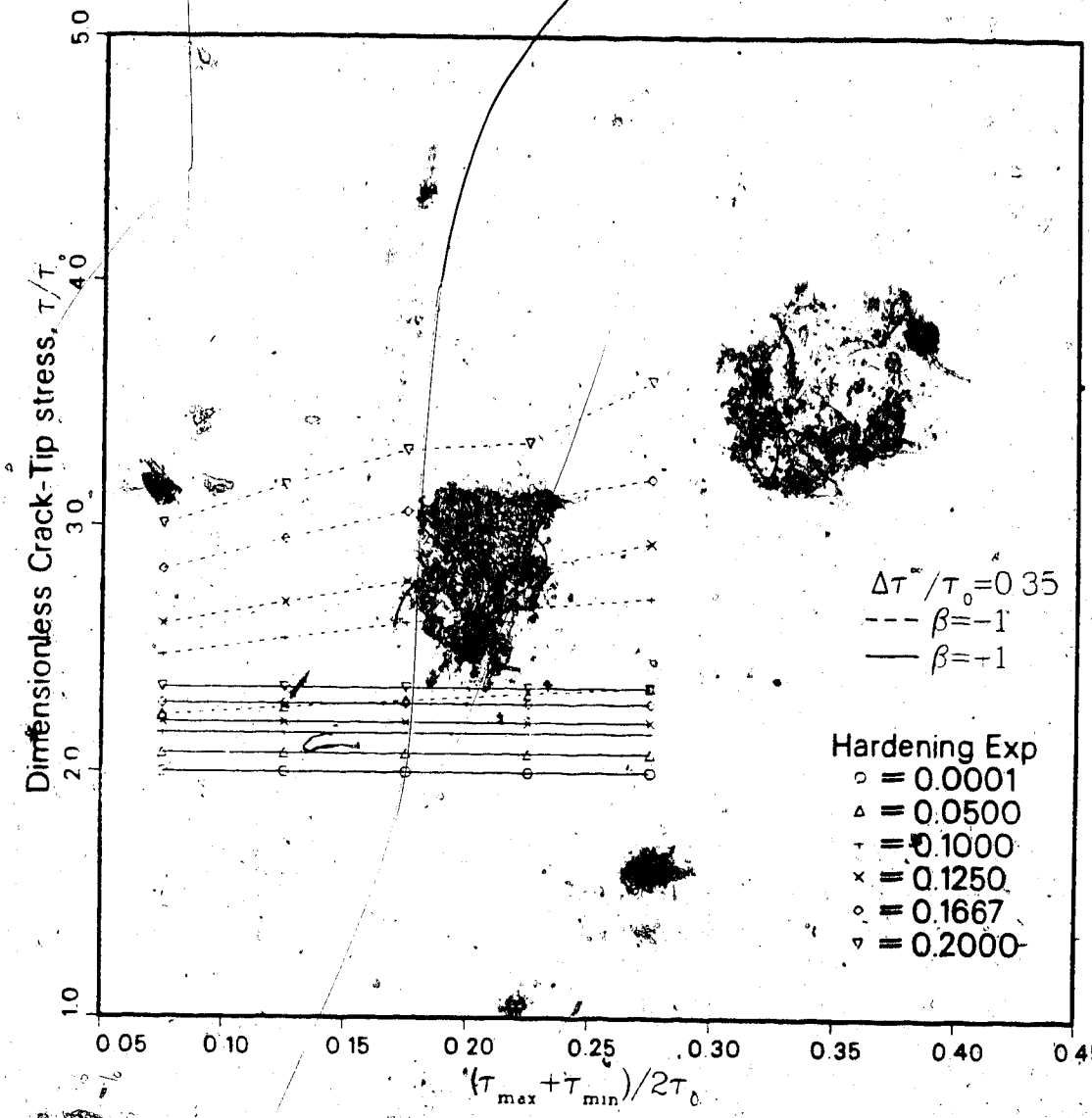

Figure 5.8 Variation of crack-tip stress range with hardening and mean applied stress

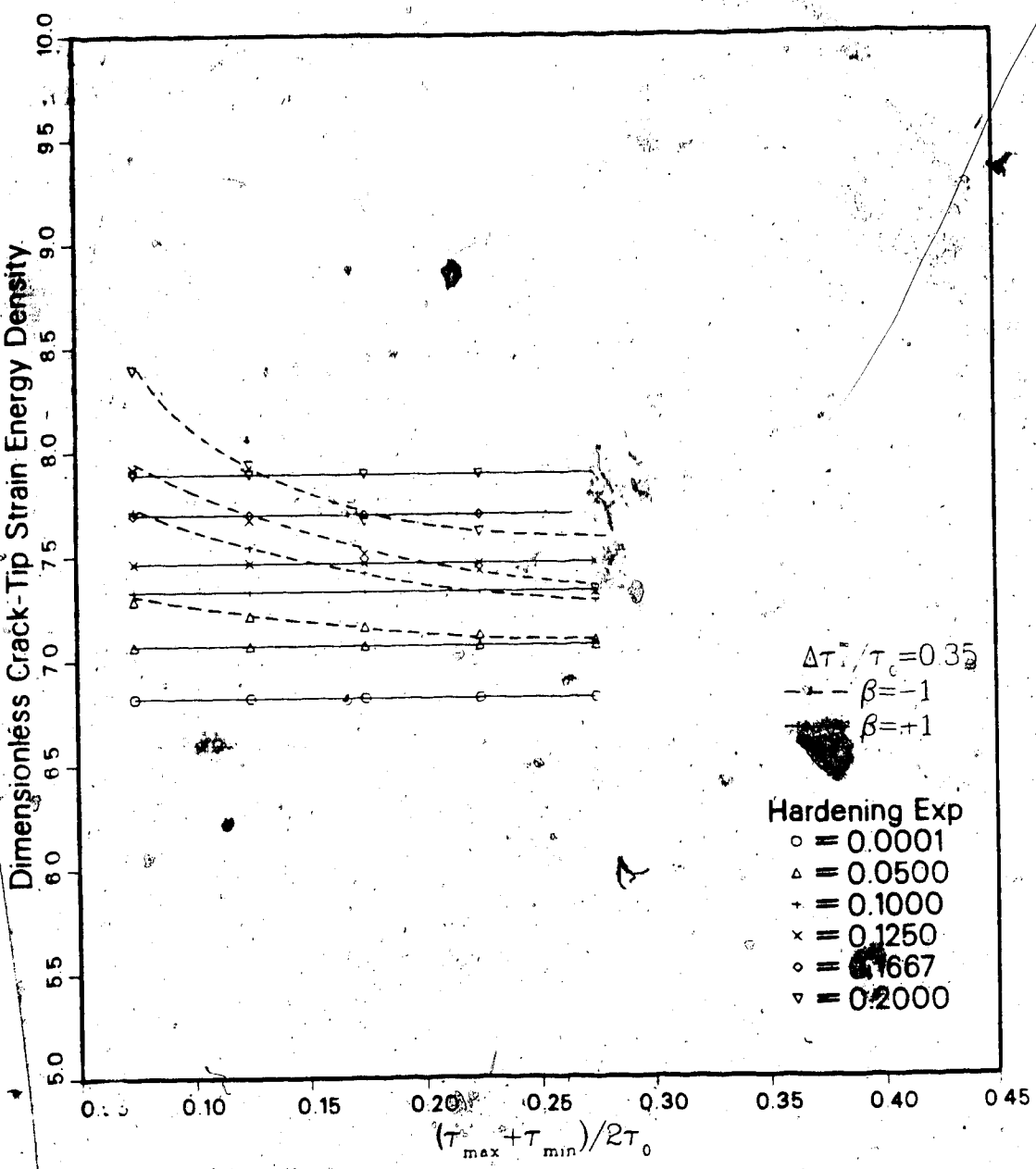

Figure 5.9 Variation of crack-tip strain energy density range with hardening and mean applied stress

hardening for both cases ($\beta = \pm 1$). Note that for the elastic-perfectly plastic case (i.e. hardening exponent, $n' = 0$) the results for all cases $|\beta| = \leq 1$ coincide as expected. In the kinematic hardening case, the variations in the displacement, J-integral and other field quantities cosidered are practically independent of the applied mean stress, while there is a decrease with the applied mean stress for the isotropic hardening case. Fig. 5.10 shows the variation of the cyclic J-integral with the applied mean stress. As in the previous case, the effect of work-hardening is to increase the cyclic J-integral. This variability is also not sensitive to the mean stress for the kinematic hardening case. However, for isotropic hardening, the cyclic J-integral increases with the applied mean stress.

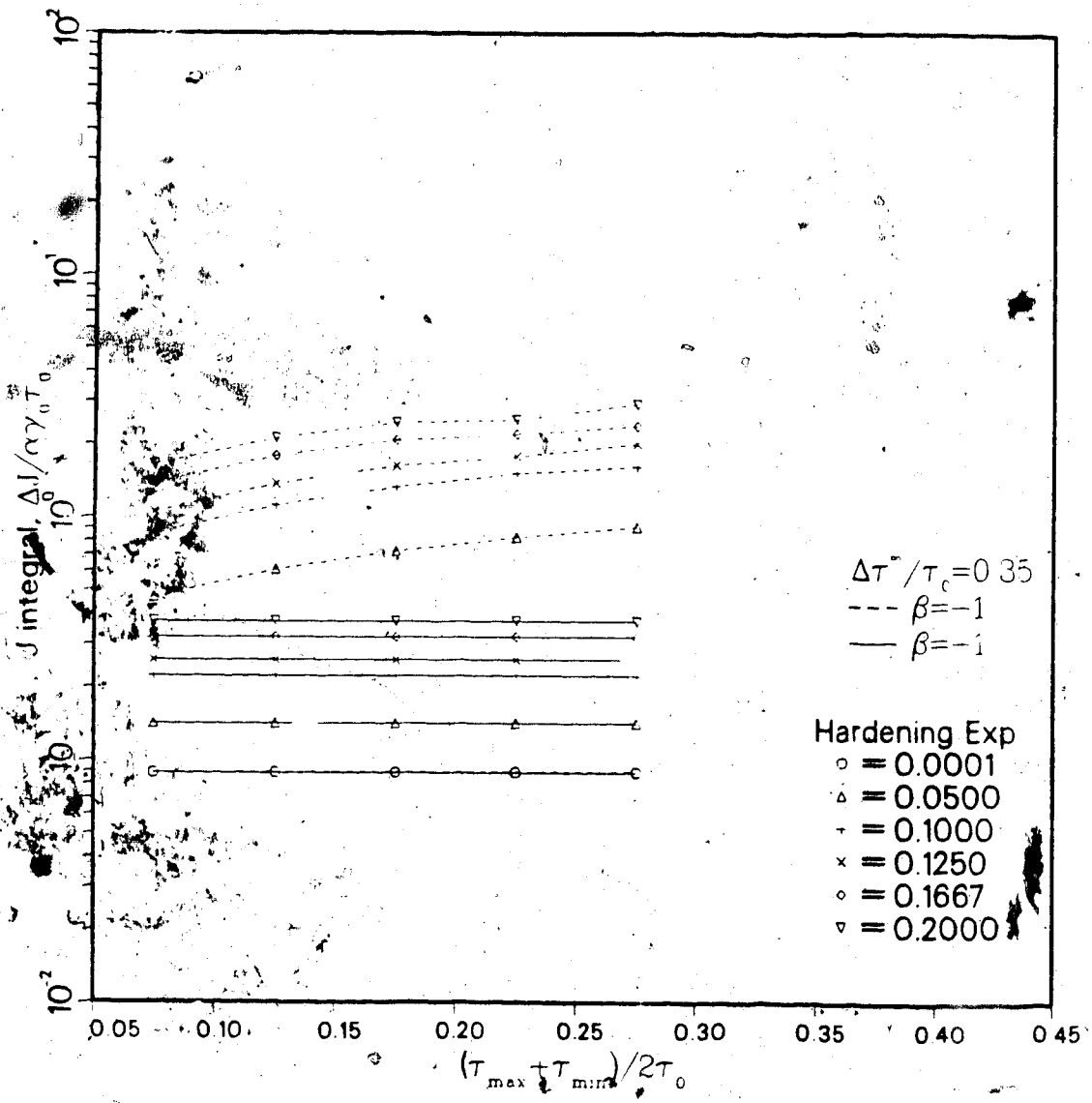

Figure 5.10 Variation of cyclic J-integral with hardening and mean applied stress

Chapter 6

DISCUSSION AND CONCLUSIONS

6.1 Deterministic Model

The main unresolved problem in the damage accumulation modelling of the fatigue crack-tip has been the treatment of the crack-tip fatigue element. Some authors (e.g. [20]) have completely ignored the damage contribution in this region, while others (e.g [21]) have considered it to be the only important aspect of damage accumulation. The seeming contradiction is resolved in the approach presented in this thesis. By including the two contributions, a crack growth rate law has been obtained that fully accounts for the total damage contribution in the fatigue damage zone. The singularity at the origin was removed by noting the experimental evidence that the stress/strain levels sustainable in the fatigue elements cannot be higher than the fatigue strength and ductility coefficients respectively. By assuming that this is attainable only at the critical value of the stress intensity factor, it was possible to determine the extent to which the plastic superposition method for deriving the cyclic stress/strain levels, can be applied. In the region immediately ahead of the crack-tip, due to non-proportional plasticity, the plastic superposition method for obtaining the cyclic stress and strain is not used. Instead of removing this region from the analysis as

in [20], it was included on the assumption that the stress/strain gradient is small, so that the cyclic stress strain levels could be taken as approximately constant as in [21]. However, unlike [21], the failure criterion was applied to this (region I) in a way cognizant of the damage already accumulated in region II (see fig. 3.1). The resulting crack growth law contains the results from the two works cited as special cases. The results from using this law (as earlier demonstrated elsewhere [44]) shows that the contribution from both regions to damage accumulation is of the same order of magnitude. The error, therefore, in ignoring either part is about a factor of 2. Considering the usual scatter in crack growth data, this may not show much significant effect. This explains why the models in [20] and [21] give similar results even through they are based upon seemingly opposite premises.

6.2 Probabilistic Simulation

The main feature that distinguishes the probabilistic simulation model presented is its capability of accounting for the damage accumulation in each fatigue element throughout its damage history. This is a departure from the earlier model by Oh [7] where the system "resets" itself after each crack advance so that the fatigue elements sort of "forget" some of the previously accumulated damage. This is not the first attempt to rectify this deficiency in the memoriless probabilistic

model. Tsurui and Igarashi [33] had earlier suggested that the fatigue element could be treated as random variables whose location factor can be taken as a function of position - in order to account for historical damage. However, there is no obvious *a priori* reason that can lead to a suitable functional form for this location factor. In our approach, the historical damage is simulated once some statistical equilibrium is attained. In this way, it becomes possible to quantify this parameter and to show that its contribution to the damage process is significant. The median growth rate obtained from this simulation has also been shown to approximate the growth rate obtained from the experimental data in some structural alloys.

No attempt was made to obtain a closed form solution for the probability distribution of the growth rate. Previous attempts at closed form crack growth distributions have led to complex densities that could not be approximated by the simple density functions used in practice. Considering the approximate nature of the several factors involved in the derivation of these distributions, it was considered more important to seek the form of the distribution function. Moreover, the inclusion of the historical damage in the model presented, significantly complicates the problem. The resulting growth rate distributions were compared to some of the commonly used density functions in the literature, using

probability plots. The resulting distributions are closer to the Log-normal density than the other two: Extreme Value and Weibull densities. A further indication of the Log-normality of the data was obtained by using a Shapiro-Wilk normality test on the logarithm of the simulated crack growth rate.

6.3 Dislocation Modelling of the Cyclic Field

The dislocation model was presented as an alternative to the unresolved problem of the unloading field. Even though the dislocation modelling of crack-tip plasticity is known to be an extreme simplification of reality, it use still gives some important results comparable to that derived from contiumum considerations. The BCS [17] dislocation model was extended to the case of work-hardening by using a friction stress (opposing the dislocation motion) in the plastic line, as a nonlinear function of strain. The functional form chosen is a modified form of the Ramberg-Osgood stress-strain law. In the unloading field, by assuming that the functional form of the friction stress is retained, work-hardening was treated in a way that allows for the inclusion of the Bauschinger effect.

The inclusion of hardening in this model shows some new insights into the use of failure criterion in crack propagation modelling. While the crack-tip displacement decreases with the hardening exponent, the crack-tip

stress follows the opposite trend. To use either as the measure of fatigue damage would lead to opposite results with respect to hardening. This justifies the use (in the crack-tip modelling used in this thesis) of the product of the stress and strain ranges as a measure of cyclic plastic damage in each fatigue cycle. This measure is closely related to the cyclic strain energy density at each point.

The work-hardening dislocation model is also suitable for the evaluation of the unloading and the cyclic J-integral. This quantity unlike the stress intensity factor used in linear elastic fracture mechanics, is dependent, not only on the range of applied far-field stresses, but also on the applied mean stress. Its dependence on the latter quantity has been found to be closely related to the way Bauschinger effect enters the analysis. For instance, in the case of the elastic-perfectly plastic material where Bauschinger effect can be ignored, as well as when the yield surface is assumed to be translated without distortion (i.e. $\beta = 1$, or kinematic hardening), the mean stress effects are negligible. However, for other values of the parameter β, the mean stresses have quite significant effects on the unloading and cyclic J-integrals, as well as other stress dependent quantities like the strain energy density. We could thus conclude, on the basis of this model, that the observed mean stress dependency well documented in the

literature, can be associated with the departure from kinematic behaviour. Even though the stable cyclic behaviour of a material is usually modelled by the kinematic yield surface, the results here show that there are certain other factors affecting cyclic material damage, that are better modelled from a non-kinematic viewpoint. This is consistent with earlier results by Ellyin and Neale [61] who showed that the yield surface in a cyclically loaded material both expands and translates.

6.4 Future Work

In the failure analysis of the fatigue elements in the statistical crack growth model in chapter 3, the use of a normal distribution was justified by asymptotic considerations. While the burden of experimental evidence supports the use of unity mean, there is no *a priori* considerations for the distribution variance. The use of the standard normal distribution in this circumstance is thus a first approximation only. Experimental and analytical investigations need to be done on the variance of the distribution used.

It would also be helpful if the results of the work-hardening unloading dislocation model of chapter 5 could be extended to the case of tensile loading. The results of the analysis presented here can be formally extended to tensile loading as pointed out by Lardner [35]. The dislocation motion into the crack-tip would then

be interpreted as a "climb" instead of the sliding explanation in the shear case. It is difficult to find similar physical explanation for the former as have been done in the latter. Several alternative models have been proposed for the tensile case. Dugdale [34], Goodier and Field [56], and Bilby and Swinden [18], models are available for the elastic-perfectly plastic loading case. It would be instructive to extend these works for the unloaded crack and the nonlinear work-hardening case.

List of References

1. Hutchinson, J.W., "Fundamentals of the Phenomenological Theory of Nonlinear Fracture Mechanics", ASME Journal of Applied Mechanics, Vol. 50, 1983, pp. 1042-1052.
2. Rice, J.R., "A Path Independent Integral and Approximate Analysis of Strain Concentration by Notches and Cracks," ASME Journal of Applied Mechanics, Vol. 35, 1968, pp. 379-386.
3. Shih, C.F., "J-Integral Estimates for Strain Hardening Materials in Antiplane Shear Using Fully Plastic Solution", Mechanics of Crack Growth, ASTM STP 590, American Society For Testing and Materials, 1976, pp. 3-26.
4. Shih, C.F. and Hutchinson, J.W., "Fully Plastic Solutions and Large Scale Yielding Estimates for Plane Stress Crack Problems", ASME Journal of Engineering Materials and Technology, Vol. 98, 1976, pp. 289-295.
5. Dowling, N.E., "Crack Growth During Low Cycle Fatigue of Smooth Axial Specimens", Cycle Stress-Strain and Plastic Deformation Aspects of Fatigue Crack Growth, ASTM STP 637. American Society For Testing and Materials, 1977, pp. 97-121.
6. Miner, M.A., "Cumulative Damage in Fatigue", ASME Journal of Applied Mechanics, Vol. 12A, 1945, pp. 159-164.
7. Oh, K.P., "A Weakest-Link Model for the Prediction of

Fatigue Crack Growth Rate", ASME Journal of Engineering Materials and Technology, Vol. 100, 1978, pp. 170-174.

8. Sih. G.C. and Madenci, E., "Fracture Initiation Under Gross Yielding: A Strain Energy Denstity Criterion", Engineering Fracture Mechanics, Vol. 18, 1983, pp. 667-677.

9. Bolotin, V.V., "Statistical Methods in Structural Mechanics", Holden Day Inc., 1965.

10. Griffith, A.A., "The Phenomenon of Rupture in Solids", Philosophical Transactions of the Royal Society", Vol. 221, 1920, pp. 163-198.

11. Paris, P.C. and Erdogan, F., "A Critical Analysis of Crack Propagation Laws", Trans ASME, Vol. 85D, 1963, pp. 528-534.

12. Ellyin, F., "A Strategy for Periodic Inspection Based on Defect Growth", Theoretical and Applied Fracture Mechanics, Vol. 4, No. 2, 1985.

13. McClintock, F.A. and Zavel, Jr., F., "An Analysis of the Mechanics and Statistics of Brittle Crack Fracture", International Journal of Fracture, Vol. 15, 1979, pp. 107-118.

14. Hunt, R.A. and McCarthey, L.N., "A New Approach to Weibull's Statistical Theory of Brittle Fracture", International Journal of Fracture, Vol. 15, 1979, pp. 365-375.

15. Harlow, D.G. amd Phoenix, S.L., "Bounds on the

Probability of Failure of Composite Materials, "International Journal of Fracture, Vol. 15, 1979, pp. 321-336.

16. Bogdanoff, J.L., "A New Cumulative Damage Model, Part I", ASME Journal of Applied Mechanics, Vol. 45, 1978, pp. 246-250.

17. Bilby, B.A., Cottrell, A.H., and Swinden, K.H., "The Spread of Plastic Yield from a Notch", Proceedings of the Royal Society, Vol. A 272, 1963, pp. 304-314.

18. Bilby, B.A. and Swinden, K.H., "Representation of Plasticity at Notches by Linear Dislocation Arrays", Proceedings of the Royal Society, Vol. A285, 1965, pp. 22-33.

19. Rice, J.R., "Mechanics of Crack-tip Deformation and Extention by Fatigue", Fatigue Crack Propagation, ASTM STP 415, American Society For Testing and Materials, 1967, pp 47-311.

20. Majumdar, S. and Mor J., "Correlation Between Fatigue and Low Cycle Fagitue Properties", Fracture Tougness and Slow Stable Cracking, ASTM STP 559, 1974, pp. 159-182.

21. Glinka, G., "Cumulative Model of Fatigue Crack Growth", International Journal of Fatigue, Vol. 4, 1982, pp. 59-67.

22. Schutz, W., "The Prediction of Fatigue Life in the Crack Initiation and Propagation Stages - a state of the Art Survey", Engineering Fracture Mechanics, Vol.

11, 1979, pp. 405-421.

23. Hult, J.A. and McClintock, F.A., "Elastic-Plastic Stress and Strain Distribution Around Sharp Notches Under Repeated Shear", Ninth International Congress of Applied Mechanics, Vol. 8, Brussels, 1956.

24. Rice, J.R. "Plastic Yielding at a Crack-Tip", Proceedings, International Conference on Fracture, Sendai, Japan, 1965.

25. Lehr, L.R. and Liu, H.W., Fatigue Crack Propagation and Strain Cycling Properties", International Journal of Fracture Mechanics, Vol. 5, 1969, pp. 45-53.

26. Challant, G. and Remmy, L., "Model of Fatigue Crack Propagation by Damage Accumulation at the Crack-tip", Engineering Fracture Mechanics, Vol. 18, 1983, pp. 939-952.

27. Antolovitch, S.D. Saxena, A. and Chanani, G.R., "A Model for Fatigue Crack Propagation", Engineering Fracture Mechanics, Vol. 7, 1976, pp. 649-652.

28. Chakrabortty, S., "A Model Relating Low Cycle Fatigue Properties and Microstructure to Fatigue Crack Propagation Rates", Fatigue of Engineering Materials and Structures, Vol. 2, 1979, pp. 331-334.

29. Head, A.K., "The Growth of Fatigue Cracks", Philosophical Magazine, Vol. 44, 1953, pp. 925-958.

30. Rice, J.R. and Rosengren, G., "Plane Strain Deformation near a Crack-tip in a Power-Law Hardening Material", Journal of the Mechanics and Physics of

Solids, Vol. 16, 1968, pp. 1-12.

31. Hutchinson, J.W., "Singular Behaviour at the end of a Tensile Crack in a Hardening Material", Journal of the Mechanics and Physics of Solids, Vol. 16, 1968, pp. 13-31.

32. Weibull, W., "A Statistical Theory of the Strength of Materials", Ing Vetenskaps Hkad Handl, No 151, 1939.

33. Tsurui, A. and Igarashi, A., "Probabilistic Approach to Fatigue Crack Growth Rate", ASME Journal of Engineering Materials and Techology", Vol. 102, 1980, pp. 300-302.

34. Dugdale, D.S., "Yielding of Steel Sheets Containing Slits", Journal of the Mechanics and Physics of Solids, Vol. 8, 1960, p100.

35. Lardner, R.W., "A Dislocation Model For Fatigue Crack Growth in Metals", Philosophical Magazine, Vol. 17, 1968, pp. 71-82.

36. Weertman, J., "Continuum Distribution of Dislocations on Faults with Finite Friction", Bulletin of the Seismological Society of America, Vol. 54, 1964, pp. 1035-1058.

37. Goldman, N.L. and Hutchinson, J.W., "Fully Plastic Crack Problems: The Centre-Cracked Strip Under Plane Strain", International Journal of Solid Structures, Vol. 11, 1975, pp. 575-591.

38. Mowbray, D.F., "Derivation of Law cycle Fatigue Relationship Employing the J-Integral Approach to

Crack Growth", Cracks and Fracture, ASTM STP 601, American Society For Testing and Materials, 1976, pp. 33-46.

39. Tanaka, K., "The Cyclic J-Integral as a Criterion for Fatigue Crack Growth", International Journal of Fracture, Vol. 22, 1983, pp. 91-104.

40. Baker, C.T.H., "Expansion Methods" in Numerical Solution of Integral Equations, L.M. Delves and L. Walsh, Editors, Claredon Press, Oxford, 1974.

41. Shih, C.F., DeLorenzi, H.G., and Andrews, W.R., "Studies in Crack Initiation and Stable Crack Growth", Elastic-Plastic Fracture, ASTM STP 668, American Society For Testing and Materials.

42 Kujawski, D. and Ellyin, F., "A Fatig. Crack Propagation Model", Engineering Fracture Mechanics, Vol. 20, 1984,pp. 695-704

43. Ellyin, F.,"The Effect of Tensile-Mean-Strain on Plastic Strain Energy and Cyclic Response", ASME Journal of Engineering Materials and Technology, Vol 107, pp.119-125

44. Ellyin, F. and Fakinlede, C., "Crack-tip Growth Rate Model for Cyclic Loading", Modelling Problems in Crack-tip Mechanics, CFC 10, Waterloo, Ontario, 1983.

45. Ellyin, F. and Li, H.P., "Fatigue Crack Growth in Large Specimens with Various Stress Ratios", ASME Journal of Pressure Vessel Technology, Vol. 106, 1984, pp. 255-260.

46. McClintock, F.A., "On the Plasticity of the Growth of Fatigue Cracks", Fracture of Solids, D.C. Drucker and J.J. Gilman, Editors, Interscience, New York, 1963, pp. 65-102.

47. Feller, W., "An Introduction to Probability Theory and its Applications", Vol. II, John Wiley, pp. 262-265.

48. Shimokawa, T. and Tanaka, S., "A Statistical Consideration of Miner's Law", International Journal of Fatigue, Vol. 2, 1980.

49. Rolfe, S.T. and Barsom, J.M., "Fracture and Fatigue Control in Structures", Prentice Hall Inc., 1977.

50. Bury, K.V., "Statistical Models in Applied Science", John Wiley, 1975.

51. Betrand, M., Lefvebre, D. and Ellyin, F., "Statistical Analysis of Crack Initiation and Fatigue Fracture of Thin Walled Tubes, Using the Weibull Law", Journal of Mecanique Theorique et Appliques, Vol. 1, 1983, pp. 49.-510.

52. Hudson, C.M., and Scardina, J.T., "Effect of Stress Ratio on Fatigue Crack Growth in 7076-T6 Aluminum-Alloy Sheet", Engineering Fracture Mechanics, Vol. 1, 1969, pp. 429-446.

53. Newman, Jr., J.D., "Finite Element Analysis of Fatigue Crack Closure", ASTM STP 590, 1976, pp. 281-301.

54. Gakhov, F.D., "Boundary Value Problems", Trans. I.N. Sneddon, Pergammon Press, New York, 1966.

55. Muskhelishvili, N.I., "Singular Integral Equations",

English Translation, Noordhoff, Groningen, Holland, 1953.

56. Mayers, D.F., "Quadrature Methods for Fredholm Equations of the Second Kind", Numerical Solution of Integral Equations, L.M. Delves and J. Walsh, Editors, Claredon Press, Oxford, 1974, pp. 64-79.

57. IMSL, International Mathematical and Statistical Library, Houston, Texas, 1982.

58. Swinden, K., "Applications of the Theory of Internal Stresses in Crystals", PhD Thesis, University of Sheffield, 1964.

59. Davidson, D. L. and Lankford, J., "Fatigue Crack Tip Plastic Strain in High Strength Aluminum alloys", Fatigue of Engineering Materials and Structures, Vol. 3, 1980, pp.289-303

60. Guerra-Rosa, L.,Moura Branco, C. and Radon, J. C., "[illegible]otonic and cyclic crack-tip plasticity", International Jou: al of Fatigue, Vol. 6, 1984 pp. 17-25.

61. Ellyin, F. and Neale, K. W., "Effect of Cyclic Loading on the Yield Surface", ASME Journal of Pressure Vessel Technology, Vol. 101, 1979, pp. 59-63.

62. Goodier, J.N. and Field, F.A., "Plastic Energy Dissipation in Crack Propagation", Fracture of Solids, D.C. Drucker and J.J. Gilman, Editors, John Wiley, New York, 1963, pp. 103-118.

APPENDIX

A1. Distribution of sums of random variables

Let X_1 and X_2 be jointly continuous random variates with the joint distribution function

$$f(x_1,x_2) \qquad \text{A1.1}$$

The random variable $Y = X_1 + X_2$ is also continuously distributed. The distribution function of the latter is,

$$F(y) = P[X_1 + X_2 \leq y] \qquad \text{A1.2}$$

$$= P[\{(x_1,x_2): x_1 + x_2 \leq y\}] \qquad \text{A1.3}$$

$$= \int\int_{\{(x_1,x_2):x_1 + x_2 \leq y\}} f(x_1,x_2)dx_1dx_2 \qquad \text{A1.4}$$

$$= \int_{-\infty}^{\infty} dx_1 \int_{-\infty}^{y-x_1} dx_2\, f(x_1,x_2) \qquad \text{A1.5}$$

$$= \int_{-\infty}^{\infty} dx_1 \int_{-\infty}^{y} dx_2' \, f(x_1, x_2' - x_1') \qquad \text{A1.6}$$

If in addition, it is known that X_1 and X_2 are independent, then,

$$f(x_1, x_2) = f_1(x_1) f_2(x_2) \qquad \text{A1.7}$$

where $f_1(x_1)$ and $f_2(x_2)$ are the individual density functions respectively. It follows from A1.6 and A1.7 that,

$$F(y) = \int_{-\infty}^{\infty} dx_1 \int_{-\infty}^{y} dx_2' \, f_1(x_1) f(x_2' - x_1) \qquad \text{A1.8}$$

Differentiating equation A1.8 leads to an expression for the density of Y, f(y) given by

$$f(y) = \int_{-\infty}^{\infty} f_1(x_1) f_2(y - x_1) dx_1 = \int_{-\infty}^{\infty} dx_1 \int_{-\infty}^{\infty} dx_2' \, f_1(x_1) f_2(x_2' - x_1')$$

$$f(y) = \int_{-\infty}^{\infty} f_1(y - x_1) f_2(x_1) dx \qquad \text{A1.9}$$

The last expression is called a convolution of the functions f_1 and f_2. This idea can be extended to the case of a random variable which is the sum of more than two random variates. Mutual independence will lead to a density function involving a convolution of the initial random variate densities.

A2. The Integral $\int_x^a R(x',y) + R(x' - y)dx'$ (Section 4.5)

Let

$$H(a,x,y) = \cosh^{-1}\left|\frac{a^2 - x^2}{a(x - y)} + \frac{x}{a}\right| \qquad \text{A2.1}$$

It has been shown by Swinden [58] that,

$$H(a,x,y) = H(a,y,x) \qquad \text{A2.2}$$

and that

$$\frac{\partial}{\partial y} H(a,x,y) = R(x,y) \qquad \text{A2.3}$$

It will be shown here that the integral,

$$\int_x^a R(x',y) + R(x',-y)dx' = K(x,y) \qquad \text{A2.4}$$

where

$$K(x,y) = \cosh^{-1}\left|\frac{a^2 - x^2}{a(x-y)} + \frac{x}{a}\right| + \cosh^{-1}\left|\frac{a^2 - x^2}{a(x+y)} + \frac{x}{a}\right|$$

$$- 2\sqrt{\frac{a^2 - x^2}{a^2 - y^2}} \qquad \text{A2.5}$$

From A2.3 it follows that,

$$\frac{\partial}{\partial x} H(a,y,x) = R(y,x) \qquad 2.6$$

Using the symmetry property (Eq. A2.2) we have,

$$\frac{\partial}{\partial x} H(a,x,y) = R(y,x) \qquad A2.7$$

and,

$$\frac{\partial}{\partial x} H(a,x,-y) = R(-y,x) \qquad A2.8$$

$$\frac{\partial K(x,y)}{\partial x} = \frac{\partial}{\partial x}\left\{H(a,x,y) + H(a,x,-y) - 2\sqrt{\frac{a^2 - x^2}{a^2 - y^2}}\right\} \qquad A2.9$$

which from the above can be written,

$$= R(y,x) + R(-y,x) + 2/\sqrt{\{(a^2 - x^2)(a^2 - y^2)\}} \qquad A2.10$$

$$= -\left\{\frac{1}{x+y} + \frac{1}{x-y}\right\}\sqrt{\frac{a^2 - y^2}{a^2 - x^2}} + \frac{2}{\sqrt{\{(a^2 - x^2)(a^2 - y^2)\}}} \qquad A2.11$$

which after some rearrangements can be shown to be

$$= - R(x,y) - R(x,-y) \qquad \text{A2.12}$$

This and the fact that $K(a,y)=0$ completes the proof.

A3. Path Independence of The Cyclic J-integral [39].

The cyclic J-integral is defined as

$$\Delta J = \int_{\Gamma} \left(\Delta W dy - \Delta T_m \frac{\partial u_m}{dx} \right) ds \qquad \text{A3.1}$$

where

$$\Delta W = \int_{(\varepsilon_{k\ell})_i}^{(\varepsilon_{k\ell})_j} [\sigma_{k\ell} - (\sigma_{k\ell})_i] \, d\varepsilon_{k\ell} \qquad \text{A3.2}$$

is the strain energy density range between states i and j, $\Delta T_m = (T_m)_j - (T_m)_i$ is the change in the traction vector, and $\Delta u_m = (u_m)_j - (u_m)_i$ is the change in the displacement vector. Consider any two paths Γ_1 and Γ_2 and suppose Γ_1 encloses Γ_2. Let ΔJ_1 and ΔJ_2 be the associated cyclic J-integrals with these paths. On the assumption that the stress and strain feilds in the enclosed region are known for an initial state i,

$$\Delta J_2 - \Delta J_1 = \int_{A(\Gamma_2,\Gamma_1)} \left\{ \frac{\partial \Delta W}{\partial x_{k\ell}} - \Delta\sigma_{k\ell} \frac{\partial \Delta\varepsilon_{k\ell}}{\partial x} \right\} dxdy \qquad \text{A3.3}$$

where $A(\Gamma_2,\Gamma_1)$ is the region contained in these curves. Green's theorem has been used to convert the line integral in Eq. A3.1 to the surface integral A3.3. Now,

$$\frac{\partial \Delta W}{\partial x} = \frac{\partial}{\partial x} \int_{(\varepsilon_{mn})_i}^{(\varepsilon_{mn})_j} \{\sigma_{k\ell} - (\sigma_k \qquad \text{A3.4}$$

$$= \frac{\partial}{\partial x}\left\{ \int_0^{(\varepsilon_{mn})_j} \sigma_{k\ell}\, d\varepsilon_{k\ell} - \int_0^{(\varepsilon_{mn})_i} \sigma_{k\ell}\, d\varepsilon_{k\ell} - (\sigma_{mn})_i (\varepsilon_{mn})_j + (\sigma_{mn})_i (\varepsilon_{mn})_i \right\} \qquad \text{A3.5}$$

Differentiating under the integral sign leads to

$$\frac{\partial \Delta W}{\partial x} = (\sigma_{mn})_j \frac{\partial (\varepsilon_{mn})_j}{\partial x} - (\sigma_{mn})_i \frac{\partial (\varepsilon_{mn})_i}{\partial x} - (\sigma_{mn})_j \frac{\partial (\varepsilon_{mn})_i}{\partial x}$$

$$- (\sigma_{mn})_i \frac{\partial (\varepsilon_{mn})_j}{\partial x} + 2(\sigma_{mn})_i \frac{\partial (\varepsilon_{mn})_i}{\partial x} \qquad \text{A3.6}$$

$$= [(\sigma_{mn})_j - (\sigma_{mn})_i][\partial(\varepsilon_{mn})_j/\partial x - \partial(\varepsilon_{mn})_i/\partial x]$$

$$= \Delta\sigma_{k\ell}\, \partial\varepsilon_{k\ell}/\partial x \qquad \text{A3.7}$$

Using A3.7 in A3.3, we obtain,

$$\Delta J_2 - \Delta J_1 = 0 \qquad \text{A3.8}$$

Hence the cyclic J-integral is path independent.